Università
Ca'Foscari
Venezia

Department of Molecular Sciences and Nanosystems

Master's Degree in
Science and Technology of Bio and Nanomaterials

Synergistic effect of Ru-doped Fe_2TiO_5: An innovative catalyst advancing Urea-Assisted water splitting efficiency

---

Supervisors
Dr. Kassa Belay Ibrahim
Prof. Alberto Vomiero

Co-supervisor
Dr. Matteo Bordin

Graduand
Mohammadhossein Hamrang
893135

Academic year
2023/2024

Table of Contents

Abstract

The process of splitting water into hydrogen and oxygen using renewable energy sources which is known as the hydrogen economy, has emerged as a promising replacement for the existing hydrocarbon economy and further using clean hydrogen as fuel. A vital approach for the hydrogen economy with zero carbon emissions is the production of hydrogen using water electrolysis. Despite all the mentioned advantages, these chemical reactions are challenging to perform due to thermodynamics limitation. Therefore, designing the catalysts to tackle these barriers is essential to speed up Oxygen evolution reaction. To settle such issue, herein, we synthesize Ru-dopped Fe_2TiO_5 via hydrothermal and chemical vapor deposition process through regulating Ru metal as a new 1D material in water splitting catalysis. The obtained electrocatalyst was characterized by XRD, SEM, EDX and XPS techniques and its catalytic activity was then evaluated by electrochemical technique. As a result, the Ru-dropped Fe_2TiO_5 exhibits outstanding catalytic performance with overpotential 230 mV (calculate at 10 mA cm^{-2}) with Tafel slope as low 92 mV dec^{-1}. To further enhance OER kinetics we use urea to assist water oxidation which is confirmed by outstanding catalytic performance with overpotential 150 mV (calculate at 10 mA cm^{-2}) with Tafel slope as low as 52 mV dec^{-1}. To confirm the material stability, we measure a chronopotentiometry at various current densities (10, 50 and 150 $mAcm^{-2}$) and the doped materials shows no drop in potential for about 36hr under UOR and show 2% drop in potential under OER. This confirms the urea use to assist water oxidation enhances the catalytic activity by drastically improve reaction kinetics as evidenced from the Tafel plot.

Finally, the improved electrocatalytic performance of the sample can be assigned to the presence of Ru atoms which can be a favorable catalytic active site and the presentence of urea that can undergoes a facile chemical decomposition compared under alkaline electrolyte and significantly speed up the reaction kinetic. This thesis offers a facile synthesis strategy for Ru-based transition metal electrocatalyst with excellent electrocatalytic efficiency towards OER and UOR.

1. Introduction

1.1 Growing importance of renewable energy sources

The continuous urbanization and growth of the world's population and economy have led to a considerable increase in energy demand. To date, around 80% of the global consumption of energy is fulfilled by fossil fuels **(Fig.1)**, which are being dwindled dramatically. However, the methods used for the extraction, transportation, processing, and most importantly, the final use of fossil fuels have detrimental effects on the environment that have an adverse influence on the economy both directly and indirectly. Coal excavation devastates the area, necessitating its reclamation and a prolonged period of inactivity. Spills and leaks that happen during the extraction, transportation, and storage of oil and gas pollute the air and water. Environmental effects are also a result of refining procedures. But most of the environmental impact of fossil fuels happens during usage that significant increase in greenhouse gases and CO_2 in the environment, causing adverse climate changes. Regardless of the ultimate goals (such as heating, producing electricity, or providing motor power for transportation), combustion is regarded as the primary reason for using fossil fuels.

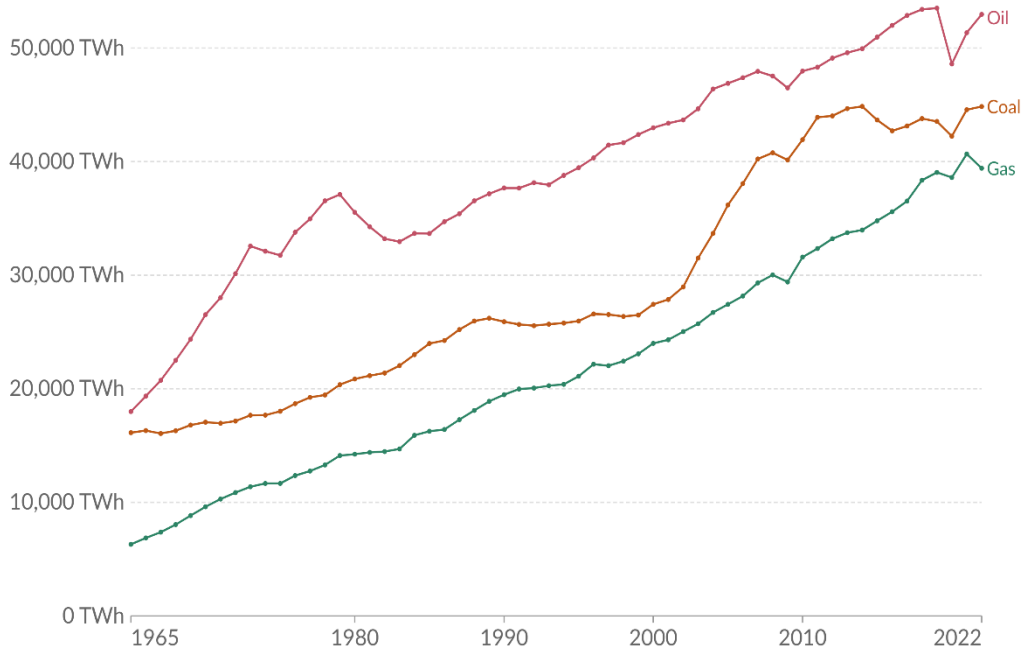

***Figure 1**. the use of fossil fuels Measured in terawatt-hours (TWh)*

Source: ourworldindata.org

Carbon and hydrogen are the main elements of fossil fuels, but they also contain a few other substances like lead and alcohols which are added during refining process. Also, some other chemicals like sulfur were originally included in the fuel. Fossil fuel combustion releases a variety of gases (CO_x, SO_x, NO_x, CH_4), soot and ash, tar droplets, as well as other organic chemicals into the atmosphere, these chemicals are also the risk factors for air pollution [1]. In this regard, **Fig.2** presents fossil fuel-related CO_2 emissions, and the growth in their consumption in 2023 all over the world.

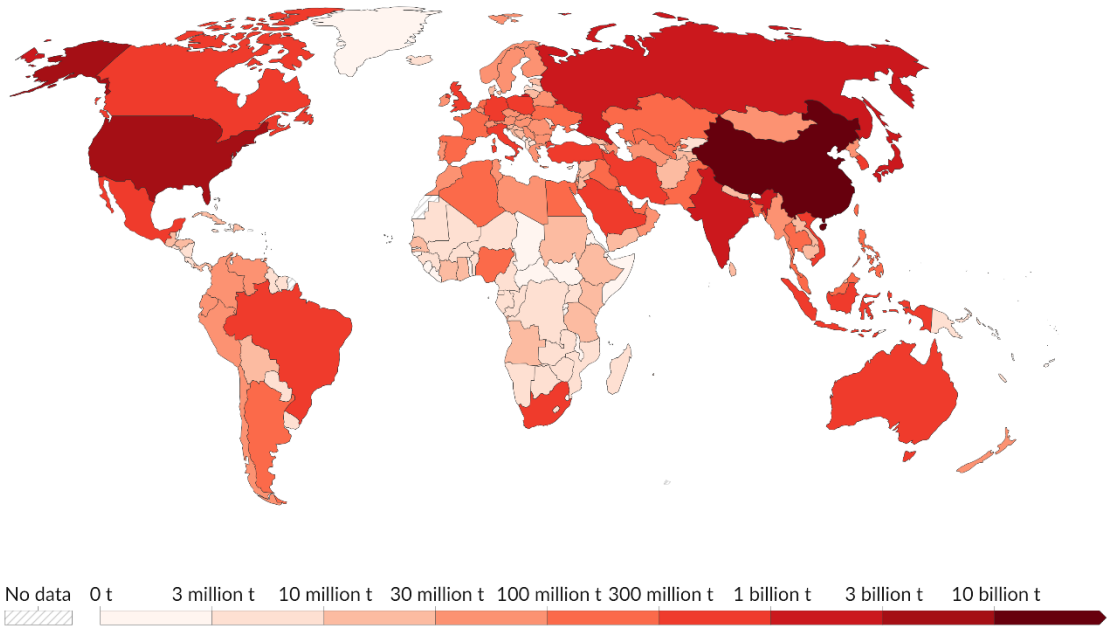

Figure 2. *Emissions of carbon dioxide (CO_2) from industry and fossil fuels*
Source: ourworldindata.org

Being within the atmosphere, these primary pollutants can engage in chemical reactions, shift into other forms, and become other contaminants like ozone, aerosols, phenoxyacid nitrates, different acids, etc. These reactions might be caused by sunlight, combining with water, or other atmospheric chemicals. We can point to the formation of acid rain because of sulfur and nitrogen oxide dissolving in clouds and rain droplets and formation of sulfuric and nitric acids.

Weak carbonic acid is produced when carbon dioxide and water are in balance; nevertheless, carbonic acid loses its acidifying properties below pH 5 [2]. Acid deposition, whether wet or dry,

harms aquatic and terrestrial ecosystems, impacting people, animals, plants, and buildings. It also causes soil and water to become more acidic.

The rest of the byproducts of combustion in the atmosphere, primarily carbon dioxide, along with other gases referred to greenhouse chemicals (nitrogen oxide, methane, and chlorofluorocarbons), absorb infrared energy that the Earth radiates back into the atmosphere, raising global temperatures which is the main reason of sea level rise, ice cap melting, climate changes, heat waves, droughts, floods, greater storms, more wildfires, etc.

Based on all the mentioned reasons limiting greenhouse gas emissions has been a top objective and a global initiative has been launched to cut greenhouse gas emissions and restrict the rise in the mean worldwide temperature to no more than three degrees Celsius over preindustrial levels [3-5]. A proved strategy for cutting greenhouse gas emissions and achieving the UN Sustainable Development Goals is hydrogen. Additionally, extensive integration of renewable energy sources (RES) is a clean, eco-friendly method of accelerating the required energy transformation [6].

Natural gas, oil, coal, and water electrolysis are the four primary methods used to produce hydrogen for commercial use. These methods produce 48%, 30%, 18%, and 4% of the hydrogen produced worldwide, respectively. The primary source of industrial hydrogen is fossil fuels. By 2020, coal gasification, partial oxidation of heavier hydrocarbons, and steam reforming of natural gas and other light hydrocarbons will provide over 95% of the world's hydrogen. Methane pyrolysis and biomass gasification are two more techniques for producing hydrogen. Any electrical source, including renewable energy sources, can be used for methane pyrolysis and water electrolysis. Each of the varieties of hydrogen fuel sources have a unique combination of benefits and drawbacks. Although the abundance and pre-existing infrastructure of natural gas and oil are positives, their main drawback is the huge amount of carbon emissions that are produced throughout their production processes. The dependence on non-renewable resources adds to the uncertainty around sustainability over the long run. Despite its abundance, coal has the same disadvantages as other fossil fuels, plus the environmental effects of mining and processing. The greatest option is water electrolysis, which produces hydrogen without emitting carbon dioxide and is especially environmentally friendly when driven by renewable energy. However, the energy-intensive nature of electrolysis and the significant infrastructure investments, require present drawbacks. Developing a hydrogen production plan that meets the difficulties presented by each

approach and is in line with environmental sustainability objectives requires striking a balance between these benefits and drawbacks.

Water splitting powered by electricity has emerged as a viable method for producing hydrogen (H_2), a clean fuel, using a significant surplus of electrical energy from renewable energy sources. Hydrogen is the energy carrier with the largest gravimetric energy density; it is also the most sustainable. Its usage as a fuel in a fuel cell not only results in high energy conversion efficiency but also in zero pollution since the only byproduct it releases is water.

$$H_2O + \text{electrical energy} \rightarrow H_2 + \tfrac{1}{2} O_2 \quad (1)$$

As a result, there is an international initiative to create fuel cells and water splitting cells for the efficient conversion of hydrogen to electricity and the manufacture of hydrogen from renewable sources. Among a variety of advances in the creation of the sustainable power package of the future, electrocatalysts, have been crucial in minimizing the kinetic energy barriers for the electrochemical reactions of hydrogen, oxygen, and water in fuel cells and water-splitting cells. This progressive route centers on the function of catalysis in electrolysis water-splitting cells [7]. Since despite all benefits associated with employing hydrogen as fuel, this process is essentially uneconomical and is only taken into consideration theoretically if catalysts are not included.

However, Water electrolysis presents issues related to efficiency, maintenance costs, robustness, reliability, and safety as well. A promising method for hydrogen production is catalysis. Several challenges confront the field of water splitting electrocatalysis. One significant hurdle is the quest for efficient and cost-effective catalysts for both the oxygen evolution reaction (OER) and hydrogen evolution reaction (HER). The expense and low efficiency of many catalysts currently impede the overall performance of water splitting systems. Additionally, catalysts must exhibit stability and durability over prolonged operation periods, as the harsh conditions, including acidic or alkaline environments and high current densities, can lead to catalyst degradation, thereby diminishing system efficiency. The sluggish kinetics of the oxygen and hydrogen evolution reactions pose another obstacle, necessitating high overpotentials to drive these reactions. Furthermore, selecting an electrolyte that is both compatible with catalysts and offers the necessary ionic conductivity while remaining stable over time proves challenging. Efficient mass transport of reactants to the catalyst surface and the transport of products away from the catalyst surface are crucial for high catalytic activity, but mass transport limitations can hinder overall performance.

Scaling up promising catalysts from laboratory settings to practical water splitting systems for large-scale applications introduces its own set of challenges. The cost of materials, particularly precious metals like platinum and iridium, can be a limiting factor for widespread adoption, necessitating the development of alternative, Earth-abundant materials to reduce costs and enhance scalability. Lastly, achieving selectivity for either the OER or HER without crossover reactions remains a challenge, requiring catalysts that exhibit high selectivity for one reaction over the other for efficient and practical water splitting. Addressing these challenges is crucial for advancing sustainable hydrogen production technologies.

To enhance electrocatalytic water splitting processes, electrocatalysts must fulfill several key criteria. First and foremost, they should exhibit high catalytic activity for both the oxygen evolution reaction (OER) and hydrogen evolution reaction (HER), enabling efficient water splitting by accelerating reaction kinetics and reducing overpotentials. Additionally, these electrocatalysts must demonstrate stability and durability over extended operational periods, resisting corrosion and degradation in harsh electrolytic conditions. Achieving high selectivity for either the OER or HER without crossover reactions is crucial to prevent the wasteful use of energy and resources. Cost-effectiveness is paramount for widespread adoption, necessitating the use of Earth-abundant materials to reduce dependency on rare and expensive elements. Ensuring efficient mass transport of reactants and products at the electrode surface maximizes catalytic activity and overall efficiency. Furthermore, compatibility with the chosen electrolyte and scalability for large-scale applications are vital considerations. Finally, a focus on environmental compatibility in both the production and utilization of electrocatalysts is essential for the development of sustainable water splitting technologies.

1.2 Hydrogen energy and electrochemistry of water splitting

Rapidly increased utilization of traditional fossil fuels and the negative environmental consequences have motivated researchers to develop advanced strategies to secure renewable and affordable energy supplies. Due to the earth-abundance, high gravimetric energy density, and carbon-free emission, hydrogen energy is a promising candidate to replace exhaustible fossil fuels. It is considered as an environmentally friendly energy vector due to its zero CO_2 and zero noxious gas emissions produced from water. Currently, most of the hydrogen gas (over 95%) is produced from fossil fuels, however, such a process induces severe environmental problems. Alternatively, water electrolysis powered by renewable energy sources (e.g., solar, wind) can produce high-purity

eco-friendly hydrogen, which is recognized as a green and sustainable technology to fulfill the hydrogen economy **(Fig.3)** [8]. Electrochemical water splitting (EWS) can produce high-purity oxygen and hydrogen gases in water electrolyzers at the anode and the cathode, respectively.

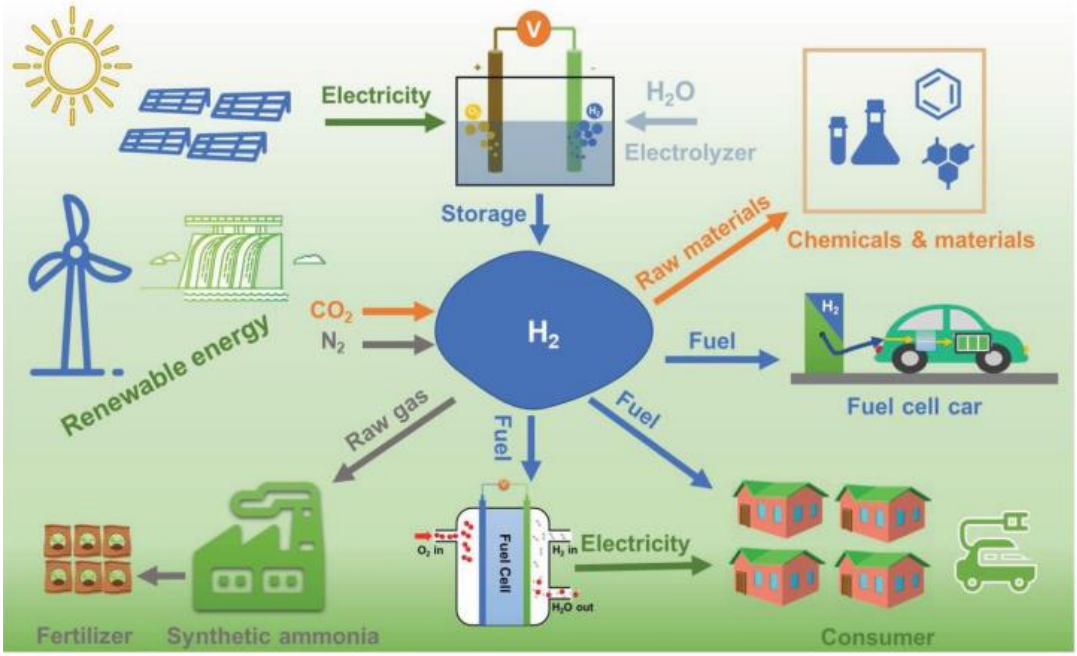

***Figure 3**. A viable route for the hydrogen economy's circulation [8].*

1.3 Water Splitting as Future Energy Carrier (H_2 Economy)

Green hydrogen production via water splitting has the potential to revolutionize the energy industry by providing efficient hydrogen production via water splitting. Nowadays, most of the hydrogen production is brought from steam reformation of hydrocarbons. However, this process is not only environmentally hazardous, but also suffers from the risk of scarcity due to non-renewable resource consumption. The production of hydrogen should be in the most spotless way to ensure its sustainability. Hydrogen gas can be eco-friendly produced by splitting water into its constituent elements, hydrogen and oxygen. Thermodynamically, the production of hydrogen from water is an uphill process that is showing following formula:

$$H_2O\ (l) \rightarrow H_2\ (g) + \tfrac{1}{2}O_2\ (g) : (\Delta G = +237\ (kJ/\ mol) \quad (2)$$

Thus, a catalyst is required that enables the dissociation of water at a faster rate. Depending on the type of external energy supply, water splitting (WS) can be catalyzed either by an external voltage (electrocatalysis). The electrocatalytic process of WS involves the decomposition of water into oxygen and hydrogen gas in response to an electric current passing through the water. It constitutes two half reactions: hydrogen evolution reaction (HER) taking place at cathode and Oxygen evolution reaction (OER) at cathode:

OER in acidic electrolyte

$$H_2O + * \rightarrow HO^* + H^+ + e^- \quad (3)$$

$$HO^* \rightarrow O^* + H^+ + e^- \quad (4)$$

$$O^* + H20 \rightarrow HOO^* + H^+ + e^- \quad (5)$$

$$HOO^* \rightarrow * + O_2 + H^+ + e^- \quad (6)$$

OER in basic electrolyte

$$OH + * \rightarrow HO^* + e^- \quad (7)$$

$$HO^* + OH^- \rightarrow O^* + H_2O + e^- \quad (8)$$

$$O^* + OH^- \rightarrow HOO^* + e^- \quad (9)$$

$$HOO^* + OH^- \rightarrow * + O_2 + H_2O + e^- \quad (10)$$

HER in acidic electrolyte

$$H_3O + * + e^- \rightarrow H^+ + H_2O \quad (11)$$

$$H^* + H^* \rightarrow H_2 \quad (12)$$

$$H_3O^+ + H^+ + e^- \rightarrow H_2 + H_2O \quad (13)$$

HER in basic electrolyte

$$H_2O + * + e^- \rightarrow H^+ + OH^- \quad (14)$$

$$H^* + H^* \rightarrow H_2 \quad (15)$$

$$H^* + H_2O + e^- \rightarrow H_2 + OH^- \quad (16)$$

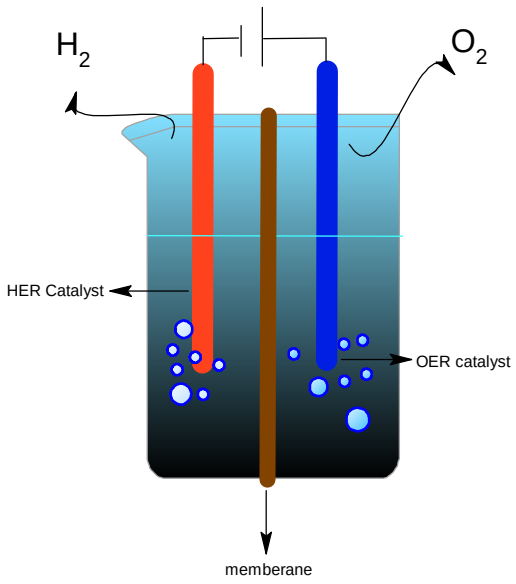

***Figure 4**. General schematic of a water electrolyzer*

HER catalysts perform well in acidic media and OER catalysts in basic ones. Integrating these catalysts to operate in the same electrolyte is challenged by pH incompatibility, resulting in inferior performance of overall WS. Furthermore, sluggish kinetics in OER has remained a grand bottleneck to realize efficient water-splitting technologies meeting the desired goals. Therefore, designing an efficient catalyst for overall WS in the same solution is crucial.

1.4 Electrochemical Water Splitting

Electrochemically, water can be heterogeneously divided in H_2 and O_2 at the surface of electrodes by providing potential across the electrodes beyond the thermodynamic potential (1.23V). During oxidation of water, electrons, protons (H^+) and molecular oxygen are produced at the anode. These protons and electrons move towards the cathode via electrolyte and external circuit respectively to complete the cycle with the liberation of molecular H_2. Generally, there are two different types of commercially available electrolyzers: **i) alkaline electrolyzers** and **ii) proton exchange membrane (PEM) electrolyzers**. The later one is highly efficient with the potential to deliver a current density of 1000-2000 mA/cm^2 but, by using highly expensive electrode materials, while alkaline based electrolyzers are assembled with transition metal-based electrode material (Ni based spinel family and perovskite) and produce comparatively low current density (20-30 mA/cm^2). Both these electrolyzers work in extremely alkaline conditions (high pH). the technical challenges, societal perception, political impact, and research opportunity are equally

important to establish such an independent energy production grid. Currently, the penetration of PV cell in the market and continuous decrease in their cost is the positive indication of this technology. However, it is equally important to improve the catalytic efficiency of electrolyzers to energetically accelerate the challenging redox reaction of water splitting process at low cost with high conversion efficiency. To address the associated problems with electrolyzers and the mediocre activity of the earth abundant materials, currently, various models have been introduced to somehow improve the water conversion efficiency. For instance**, i) overall water splitting process**, **ii) decoupled water splitting process**, **iii) hybrid water splitting approach** and **iv) tandem water splitting approach** are the newly introduced models in this regard [9].

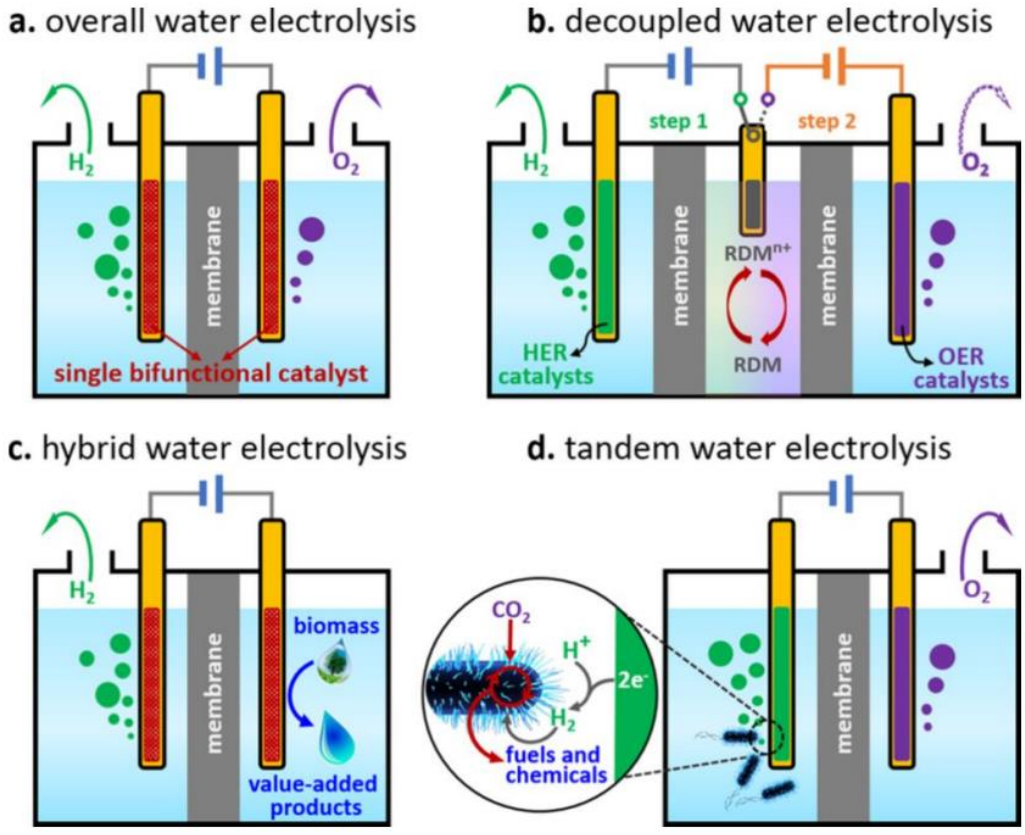

Figure 5. *Schematic illustration of various electrochemical water splitting modules (a) overall water splitting catalysis using bifunctional electrode materials (b) decoupled water splitting scheme with redox mediator (RDM) (c) hybrid water splitting scheme with catalysis of biomass (d) tandem water splitting scheme for the direct utilization of H_2 with consumption of CO_2 [9].*

Nonetheless, the sluggish anode OER results in increased energy consumption and operational costs. Specifically, although the equilibrium potential of overall water electrolysis is 1.23 V vs. RHE, the applied voltage in practical terms is elevated to 1.8-2.0 V to ensure an adequate thermodynamic driving force.

Two primary strategies have been employed to address these challenges. Firstly, there is an emphasis on developing highly efficient catalysts. Secondly, an alternative approach involves replacing the OER with more thermodynamically favorable reactions. various alternative reactions, including the oxidation of substances like ammonia, hydrazine, alcohol, glucose, and urea, have demonstrated effectiveness in facilitating water splitting with low overpotential and energy input. Notably, urea stands out as a promising candidate due to its attributes. Urea serves as a good hydrogen carrier with a high hydrogen content of 6.67 wt%. Additionally, the non-toxic products of nitrogen (N_2) and carbon dioxide (CO_2) resulting from urea oxidation reaction (UOR) prevent the simultaneous production of H_2 and O_2. Crucially, the theoretical voltage required for urea electrolysis is only 0.37 V vs. RHE, significantly lower than the 1.23 V needed for conventional water splitting. Therefore, the exploration of Earth-abundant and cost-effective materials are strongly hunted [10].

1.5 Role of electrocatalysts in water splitting

The positive value of ΔG (Gibbs free energy) indicates that electrolytic water splitting is not just an uphill process but also has to overcome an enormous kinetic barrier **(Fig.5** [11]**)**. A key factor in decreasing the kinetic barrier is catalysts. To lower the overpotential and boost the effectiveness of the water electrolysis process, the catalyst is essential [12]. Therefore, it is obvious that the electrocatalytic water splitting is not a spontaneous reaction in the absence of electrocatalysts and this is the reason that these concepts have never been two separated topics.

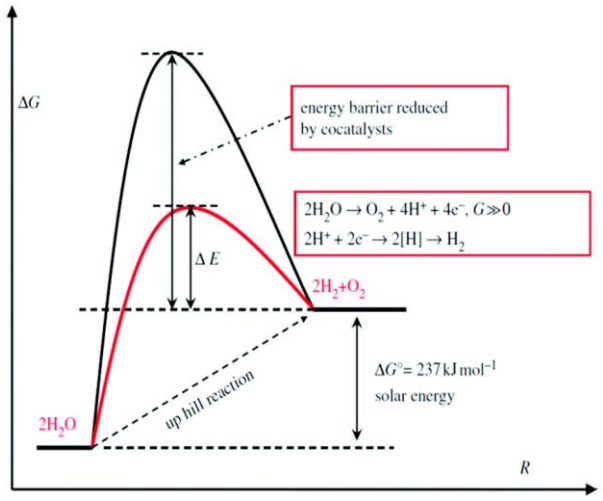

***Figure 6**. A schematic representation demonstrating how the catalyst lowers the activation energy barrier [11]*

A catalyst's effectiveness in electrocatalytic water splitting is assessed using several critical factors including activity, stability, and efficiency. The polarization curves may be used to determine the overpotential, Tafel slope, and exchange current density that characterize the activity. The variations in the overpotential or current over time define stability. The effectiveness is determined by comparing the theoretical predictions with experimental findings through the employing of the faradaic efficiency and turnover frequency. During recent years many attempts have been made to find the best chemical compounds to fulfilling all expectations from a catalyst.

Due to their high electroactivity and good stability across a wide pH range, precious metals (such as Pt, Pd, Ir, Ru, and Rh) were first thoroughly studied as catalysts for OER and HER [13-15]. However, the limited availability and excessive expense of these noble metals severely restrict their wide-scale utilization. Therefore, creating inexpensive catalysts is essential to the development of environmentally conscious hydrogen energy. As a result, several transition metals like Fe, Mn, Co, Ni, Cu, and Mo with earthly abundances have been generated to overcome these problems. Additionally, it is asserted that creating affordable electrocatalysts from natural resources is a productive means of achieving the eco-designed goal by lowering the high cost and detrimental environmental effects of the conventional catalyst preparation process, which entails the intricate procedures [16-18].

It should be mentioned that by carrying out subsequent treatment like calcination and doping and the tuning the internal and exterior properties of natural minerals, their catalytic efficiency can be greatly improved. As a result of the mentioned above, great attention to minerals containing transition metals like metal oxides and practical post treatments could be considered as a strategy to eco-designed electrocatalysts.

1.6 Urea assisted water splitting

Nowadays, molecular structure of urea has garnered significant interest in energy applications due to its potential as a hydrogen carrier for direct integration into fuel cells. Urea proves stable and more readily available compared to other liquid fuels. Furthermore, urea electrolysis, as opposed to water electrolysis, is deemed more efficient and energy-conserving. Under standard conditions, the thermodynamic voltage required for urea electrolysis is 0.37 V, significantly lower than that for water electrolysis (1.23 V). The substantial utilization of urea holds promise in curbing environmental pollution, considering that 2 to 2.5% of urea is generated from industrial wastewater.

Urea exhibits favorable oxidation thermodynamic properties, with the UOR serving as the foundational process dictating the performance of modern urea-based energy conversion technologies. It represents a pivotal half-reaction influencing the technical efficacy of urea electrolysis [19-21].

UOR reaction in Anode

$$CO(NH_2)_2 + 6OH^- \rightarrow N_2 + 5H_2O + CO_2 + 6e^- \quad E = -0.46\ V\ vs.\ SHE \qquad (17)$$

HER reaction in Cathode

$$6H_2O + 6e^- \rightarrow 3H_2 + 6OH^- \quad E = -0.83\ V\ vs.\ SHE \qquad (18)$$

Overall reaction

$$CO(NH_2)_2 + H_2O \rightarrow N_2 + 3H_2 + CO_2 \quad E = 0.37\ V \qquad (19)$$

Furthermore, in comparison to the hydrogen (H_2) created by the cathode process, the oxygen (O_2) produced on the anode is often insignificant. Thus, substituting more readily oxidized soluble molecules and thermodynamically advantageous reactions, like the urea oxidation reaction (UOR: 0.37 V), for anodic OER (thermodynamic potential: 1.23 V) [22-25] lowers the additional electricity

consumption. Also Considering urea has a high energy density as a hydrogen storage material, urea-based reactions have garnered a lot of attention as a replacement to OER for traditional water splitting. Furthermore, nontoxic nitrogen (N_2) and carbon dioxide (CO_2) are produced as byproducts of the electrolysis of urea in conjunction with the creation of H_2, thereby averting the explosion of H_2/O_2 gas combinations [26].

The urea-assisted water splitting, as mentioned above, comprises the anode oxidation of urea molecule and the cathode hydrogen evolution reaction. Compared to the HER, the UOR also faces the hindrance of slow reaction kinetics because of the 6 e^- transfer process, thus highly efficient catalysts are greatly in need to accelerate the catalytic kinetics [27,28]. The noble metal-based catalysts like Pt, Ru, exhibit considerable catalytic activity but are restricted by the cost and reserves.

Luckily, the transition metal (Co, Fe, Mn, etc.) based electrocatalysts have modest activity for UOR. Because of their earth abundance, high stability in the strong alkaline media, and the facile active phase formation resulting from the multivalent oxidation states, these catalysts for UOR have received increasing attention. To the best of our knowledge, the Iron-based catalysts can be classified into rigid substrate supported catalysts and powder catalysts, according to their states.

Moreover, the environmental significance of urea cannot be overlooked. Urea is a common environmental pollutant discharged from various sources such as agricultural fertilizer, industrial production, and domestic excretion. Therefore, harnessing urea-assisted water splitting not only yields clean hydrogen energy but also contributes to the mitigation of environmental pollution. This dual benefit underscores the potential of urea as a valuable resource in the pursuit of sustainable and environmentally friendly hydrogen production.

Despite all the mentioned advantages, the initial reaction kinetics of urea oxidation are sluggish due to a six-electron transfer process at the anode. Consequently, the quest for more efficient catalysts becomes imperative to enhance the catalytic activity and stability of urea oxidation Among various earth-abundant catalysts studied for urea-assisted water electrolysis, Pseudobrookite based materials are considered as one of the most promising candidates.

1.7 Pseudobrookite (Fe_2TiO_5) a Promising Material

Since iron titanate (Fe_2TiO_5) is an inexpensive, abundant, and non-toxic oxide with ideal electrical, optical, and chemical characteristics for this use, it has gained attention as a potential material for the next generation of water splitting. In recent years, the most attention regarding the use of Fe_2TiO_5 has been in the field of photocatalytic water splitting due to favorable band gap of 2.2 eV, allowing wide absorption of visible light, good aqueous stability, low cost, abundance in nature and long-term chemical stability in aqueous media. Pseudobrookite Fe_2TiO_5 is a reddish brown to ochre-yellow colored mineral that was first described by Pauling [29] in 1930. The orthorhombic crystal form of Pseudobrookite Fe_2TiO_5 typical Cmcm space group of ferric pseudobrookite is comprised of TiO_6 and FeO_6 octahedral geometries, forming an orthorhombic unit cell. This orthorhombic symmetry (Cmcm space group) is represented with a general formula of X_2YO_5, with X and Y being usually Fe (2 + and 3 +), Mg, Al, and Ti.

Incorporation of Fe and TiO_2 to effectively tailor band gaps based on the stoichiometry of mixed oxide. A mixed iron titanate showed better band positions than hematite. Since the valence band level for the latter was already favorable for water oxidation, the shift in conduction band level toward hydrogen generation would be expected to improve the performance. Since water reduction level (E_{H2}) is 4.5 eV with respect to Evac, it shows the conduction band (ECB) lies in the region of hydrogen generation **(Fig.7)** [30]. Through Tauc plot analysis, the band gap was evaluated to be around 2.1 eV. Hence, seems the band levels of Fe_2TiO_5 straddle the oxidation/reduction levels of H_2O.

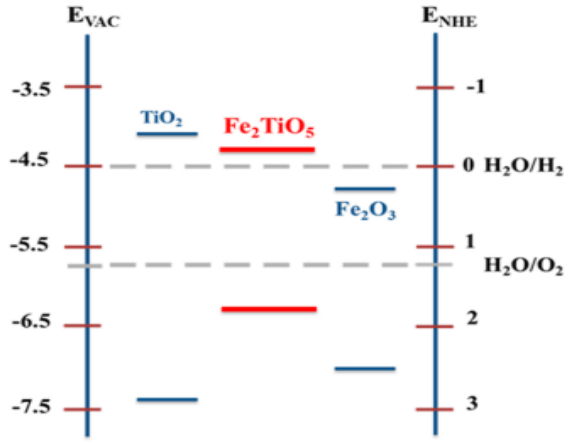

Figure 7. schematic representation of possible band level positions for Fe_2TiO_5 with respect to water redox levels [30]

Fe_2TiO_5 has undergone a number of modifications, including substrate modification, doping, cocatalyst loading, and heterojunction assembly, to improve its performance in photo(electro)chemical water splitting and herein based on these possibilities we tried to improve its electrocatalytic performance by Ru doping.

1.8 Crystal, optical, and electronic structure properties of Fe_2TiO_5

Ferric pseudobrookite (Fe_2TiO_5) exhibits an orthorhombic unit cell comprised of TiO_6 and FeO_6 octahedral configurations within the typical Cmcm space group at room temperature (**Fig. 8**). The initial elucidation of the pseudobrookite Fe_2TiO_5 crystal structure in 1930 by Pauling established its orthorhombic nature. Subsequent investigations in the literature focused on the specific positions of Fe and Ti atoms. Wyckoff [31] proposed a solid solution for ferric pseudobrookite, envisioning a fully ordered orthorhombic structure where Fe^{3+} and Ti^{4+} occupy the 8 f and 4c sites, respectively. Numerous studies utilized neutron diffraction and Mössbauer spectroscopy to probe the configurations of Fe^{3+} and Ti^{4+} ions in octahedral cells. The prevailing consensus points to a configuration where both Fe^{3+} and Ti^{4+} species share the 8 f and 4c sites, with a tendency for iron to occupy the 4c sites and titanium the 8 f sites. In recent decades, Fe_2TiO_5 has garnered attention in the magnetic materials community due to its spin glass-type short-range magnetic order characterized by uniaxial anisotropy. This compound, classified as an insulating magnetic system, exhibits a magnetically disordered state arising from the partial occupancy of metallic sites by Fe^{3+} ions and nonmagnetic Ti^{4+} ions while maintaining stoichiometry.

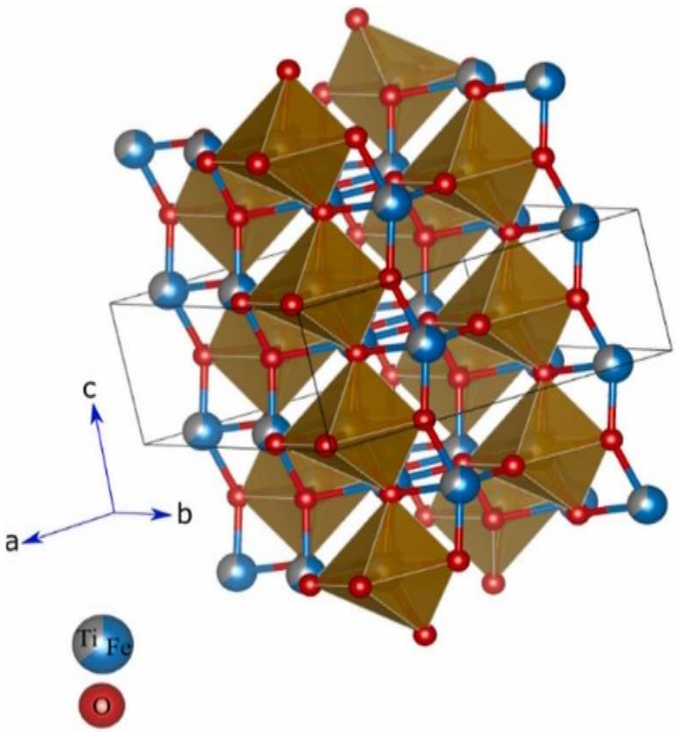

***Figure 8**. pseudobrookite Fe2TiO5 structure that is orthogonally oriented with respect to the b cell axis [29].*

The optical properties of Fe_2TiO_5 pseudobrookite are related to its interaction with electromagnetic radiation, particularly in the visible and near-infrared regions of the spectrum. These properties are influenced by the crystal structure and the electronic transitions that occur within the material. The compound's optical behavior can be characterized by studying phenomena such as absorption, reflection, and transmission of light. Detailed spectroscopic analyses, including techniques like UV-VIS spectroscopy, can provide insights into the electronic transitions occurring in Fe_2TiO_5, shedding light on its optical properties and absorption characteristics.

The electronic structure of Fe_2TiO_5 is a key factor influencing its magnetic and electrical properties. This compound is known for its spin glass-type short-range magnetic order with uniaxial anisotropy. The electronic configuration of Fe^{3+} and Ti^{4+} ions within the crystal lattice dictates magnetic behavior. Fe^{3+} ions, being magnetic, contribute to the overall magnetic properties of the material, while Ti^{4+} ions, being nonmagnetic, play a role in maintaining the compound's stoichiometry. The partial occupancy of metallic sites by Fe^{3+} ions and nonmagnetic Ti^{4+} ions lead to a magnetically disordered state.

1.9 Fe_2TiO_5 for photo(electro)chemical water splitting

Fe_2TiO_5 materials emerges as a promising mixed metal oxide material in the pursuit of advancing photo-electrochemical water splitting an innovative process harnessing sunlight. This compound boasts advantageous optical properties, featuring a bandgap conducive to absorbing light across the visible and near-infrared regions of the electromagnetic spectrum, where a substantial portion of solar energy resides. Moreover, pseudobrookite exhibits photoelectrochemical activity, a pivotal characteristic enabling the generation of electric current upon exposure to light a fundamental step in converting solar energy into chemical energy during water splitting. Renowned for its chemical and structural stability, pseudobrookite demonstrates resilience against harsh conditions, including corrosive electrolytes, essential for prolonged applications. Further bolstering its suitability, the material comprises abundant and cost-effective elements Fe and Ti contributing to the feasibility of large-scale production. Notably, the tunable properties of pseudobrookite, achievable through adjustments in synthesis conditions and element doping, allow researchers to fine-tune its performance for specific applications, notably enhancing photoelectrochemical water-splitting efficiency. Recently, Fe_2TiO_5 has been demonstrated to be able to act as a proper co-catalyst on Fe_2O_3 to improve the charge-transfer efficiency at the electrode/electrolyte interface [32].

Additionally, the material may exhibit catalytic activity in crucial reactions, such as the OER or HER, further enhancing the overall efficiency of the water-splitting process. It is imperative to recognize that ongoing research in the realm of electrochemical water splitting continues to explore diverse materials to improve efficiency and address associated challenges, with pseudobrookite Fe_2TiO_5 standing as a notable contender with promising properties for this transformative application.

To harness Fe_2TiO_5 as an effective electrocatalyst for water splitting, the critical modification of its electronic structure through metal doping is imperative. Introducing metal atoms transforms them into active surfaces conducive to water oxidation. Various transition metals, such as Mn, Ni, Co, Ru, Ir, and Mo, play a pivotal role in altering the electronic structure of Fe_2TiO_5, rendering them active sites for catalyzing water oxidation. Among these metals, Ru doping stands out as particularly noteworthy. Not only does metal doping modify the electronic structure of pseudobrookite, but it also significantly enhances catalytic activity, especially in the OER a pivotal step in generating oxygen from water. The benefits of metal doping transcend catalytic prowess,

encompassing improvements in stability, facilitation of electron transfer, tunable properties, and enhanced reaction kinetics. Ruthenium doping contributes to the stability of pseudobrookite during electrochemical reactions, meeting the crucial demand for materials enduring repeated cycles of oxidation and reduction. Additionally, doping promotes efficient electron transfer, elevating the overall conductivity of the material as an indispensable trait for high-performance electrocatalysts. The tunable properties achieved through metal doping Fe_2TiO_5 empower researchers to optimize its electronic structure and surface characteristics, tailoring the material to exhibit superior electrocatalytic activity. Furthermore, the impact of metal doping on reaction kinetics holds the potential for accelerated rates, culminating in more efficient water-splitting processes. Consequently, the diverse advantages conferred by metal doping position it as a promising element for augmenting the electrochemical performance of Fe_2TiO_5 in the realm of water-splitting applications. Here we design Ru doped Fe_2TiO_5 structure for electrochemical water oxidation.

1.10 Ruthenium (Ru) Doping

Enhancing the electrocatalytic activity of catalysts for water splitting requires foreign atom doping and according to reports, metal doping is a useful tactic for altering catalysts' electrical structure to maximize the binding strength with intermediates and improving the catalytic activity [33,34]. Choosing the right electrocatalyst is crucial to improve the electrocatalytic performance in different manners like lowering the overpotential in water splitting process. Nobel-metal based electrocatalysts have been noticed as the most promising material to fulfill this aim but due to their high cost and limited natural supplies their practical usage is impeded [35-38]. Thus, more focus should be placed on the identification and creation of affordable nanomaterials, like transition metal. Nevertheless, because of their poor electronic conductivity and inadequate intrinsic activity, these electrocatalysts continue to provide significant implementation challenges. Because of this a great deal of work has been put into improving electrical conductivity and electrocatalytic activity through efficient electronic structure modification [39-41]. Among the diversity of dopants, Ru is proving to be a perfect one to boost the electrocatalytic capacity for water splitting by altering the electrical structure, adding greater electrical conductivity, the creation of more active sites, and a potent synergistic action. Due to these benefits, Ru-doped nanomaterials have been studied extensively and used as cutting-edge water splitting electrocatalysts [35]. Recent advancements in the field of electrocatalysis highlight the significance of Ru atoms as dopants for modifying

electronic structures and enhancing electrical conductivity. This improvement is crucial for boosting the OER performance in electrocatalysts. Ru's robust OER activity is attributed to Ru–O moieties during electrooxidation [42]. Ru-doped electrocatalysts serve as additional active centers for OER, with the added advantage of encouraging the synthesis of Ru-dopped materials. This dopped material exhibit a powerful synergistic effect, further elevating electrocatalytic water splitting. Consequently, the development of Ru-doped nano catalysts holds promise for advancing water electrolysis technology.

Nano catalysts with Ru-doped structure can be synthesized through the incorporation of Ru atoms into precursors, followed by post-treatment modifications such as calcination. These catalysts exhibit outstanding electrocatalytic activity. Xu and colleagues [43] demonstrated the potent synergistic effect of Ru-doped heterostructured oxides, particularly in enhancing the OER (Oxygen Evolution Reaction) performance. Specifically, using ZIF-67 nano cubes as templates, they produced $CoMoO_4$–$Co(OH)_2$ through ion exchange between MoO_4^{-2} and 2-MIm. Alternatively, a standard wet-chemical procedure can be employed to create Ru-doped $CoMoO_4$–$Co(OH)_2$, which can then be annealed in an air atmosphere to yield $CoMoO_x/CoO_x/RuO_x$ hollow nano boxes.

In comparison to pristine $CoMoO_x/CoO_x$ with an overpotential of 250 mV at 10 mA cm^2, the CoMoOx/CoOx/RuOx hollow nano boxes exhibit significantly enhanced OER activity due to their unique compositional and structural advantages. Mechanistic research, combined with experimental data, suggests that the strong electron interaction on well-defined nanointerfaces promotes efficient electron transfer within the multi-component $CoMoO_x/CoO_x/RuO_x$ Nano boxes during OER. Additionally, the substantial synergistic effect resulting from Ru doping optimizes the binding strength with intermediates, further improving OER performance.

As a result of all mentioned above, we chose this topic to investigate and assess the feasibility and efficiency of utilizing Fe_2TiO_5 as an electrocatalyst for the electrochemical water splitting process and characterization of the electrocatalytic properties of Fe_2TiO_5 and evaluation of its performance in promoting the OER during water electrolysis. The research will involve the synthesis and modification of Fe_2TiO_5 via foreign metal doping (Ru), followed by a comprehensive analysis of its electronic, structural, morphological, and compositional properties. The electrochemical behavior of Fe_2TiO_5 will be systematically studied using various techniques, including Linear sweep voltammetry, chronoamperometry, and electrochemical impedance spectroscopy. The goal

is to provide valuable insights into the catalytic activity, and stability of Fe_2TiO_5 as an electrocatalyst for urea assisted water splitting, contributing to the broader understanding of materials suitable for sustainable and cost-effective hydrogen production through electrochemical means.

2. Outline of the thesis and objectives

The main aim was the exploration of the electrocatalytic properties of Ru-dopped Fe based catalyst to develop and design a novel nano-based system for clean energy production in water splitting. Fe-based nano catalyst was the main point of this thesis due to their easy synthesis procedure, abundancy, financial aspects and their importance in scientific field as a promising approach to fulfilling future demands of energy. As mentioned before, the catalytic activity is directly related to the final composition and morphology, therefore the main challenge was to synthesis nano catalyst with desired composition and morphology.

From primary steps, I focused from one side on the synthesis and fabrication of Fe_2TiO_5 electro catalyst. To achieve this aim, I initiated the synthesis of this material utilizing a solvothermal approach, followed by calcination. Then I modify the surface and structure using Titanium(IV) isopropoxide and Iron nitrate as a precursor.

Through the procedure steps, tailoring the time and temperature of the calcination led to optimize the synthetic procedure. On the other hand, I focused on doping step which was the most challenging part because of the high price of Ru precursor ($RuCl_3$). My aim was to minimize the use of this precious metal, but taking advantage of its properties to enhance the catalytic activity of my material. Finally, based on deep physical and chemical characterization this aim was obtained.

Fe based catalyst was chosen in this study for its low cost compared to the other precious metals. Unlike most recent studies in this field and using expensive precursor like Ru to fabricate catalysts, I tried to use Ru in a minimum level just as a modifier of electrocatalytic properties not as the main catalyst. In different stages I also had a great attention to green chemistry fundamentals. As an example, even after obtaining results, I repeated the synthesis at lower T and all the mentioned T can be considered as the lowest possible T to obtain desired composition. Scientifically all the

demands that I was expected was obtained. As a result, it could be considered as a novel protocol to producing the low-cost catalysts for water splitting and carbon free prospective.

3. Experimental section

3.1 Materials

Deionized water**,** Milli-Q water (Milli-Q, H_2O)**,** Ethanol (EtOH, sigma-Aldrich), Iron (III) nonahydrate (sigma-Aldrich), Titanium(IV) iso propoxide,2-propanol ((CH3)2CHOH), 99.9%, sigma-Aldrich) Ru(III) chloride hydrate ($RuCl_3xH_2O$, sigma-Aldrich), Ni foam (NF, thikness:1mm, Sheng Qiang co., Ltd. Jiangsu, China), Urea (NH_2CONH_2)**,** Potassium hydroxide (KOH, sigma-Aldrich), Nafion ($C_9HF_{17}O_5S$, Merck)

3.2 Synthesis

The synthesis of Fe_2TiO_5 was achieved through a solvothermal procedure according to a previously reported work [44]. As the first step, 2.51mmol of Fe $(NO_3)3.9H2O$ was completely dissolved in 50 ml of isopropanol. After that, 1.25mmol of Titanium isopropoxide was added to previous solution. Addition should be made after dissolution is complete. This solution was kept under stirring for 1h then transferred to a Teflon line stainless steel autoclave. A 150ml of Teflon was used for this purpose. Then autoclave was put in hydrothermal oven and heated at 150 ^oC for 12h with the 10 ^oC/min heating rate. After hydrothermal completion and cooling down, the obtained suspension was centrifuged, washed 3 times with deionized water (DI) and ethanol and let dried overnight at 70 °C. The sample was then calcinated in muffle. In this stage, different time and calcination T was chosen to optimize the synthesis and to obtain desired composition. The calcination was performed at 500, 600, 700, 800 and 900 ^oC for 2 and 3h for each sample.

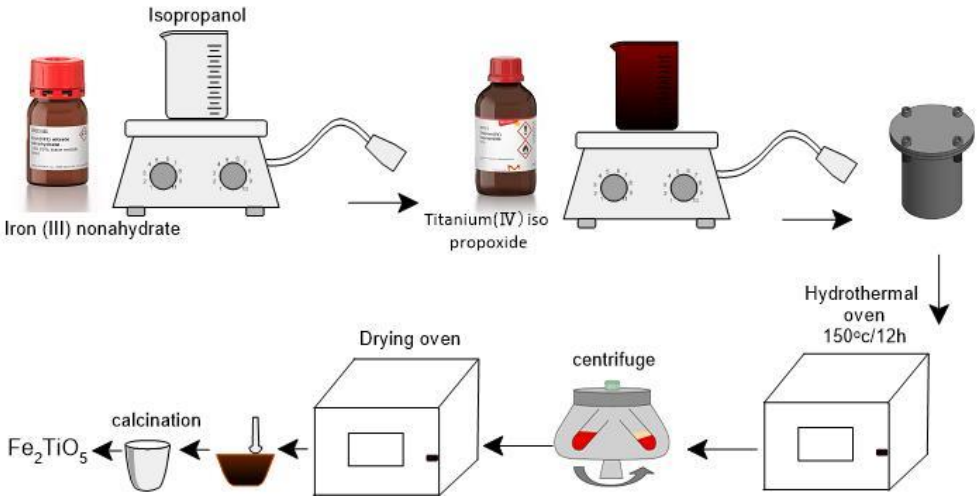

***Fig 9**. schematic representation of Fe2TiO5 synthesis procedure*

The second step was doping. In this stage, at first 0.04 g of $RuCl_3$ was dissolved in 10 ml of pure ethanol under stirring for 3h, after 3h 20 ml of DI was added to solution with 1.2 g of Fe_2TiO_5 (RuCl3:Fe2TiO5, 1:3) and was stirred for 3h. The final solution then was transferred to a 50ml Teflon and was placed to hydrothermal oven at 150 °C for 12h. The final suspension was centrifuged and washed 3 times with DI and dried at 70 °C overnight. Finally, the black obtained powder was placed in CVD setup and calcinated in Ar at 300 °C for 2h.

3.3 Materials characterization

To ensure accuracy in synthesis and understand the structural, morphological and optical properties, we used various analytical techniques to characterize the synthesized samples.

X-ray diffraction (XRD) analysis was executed utilizing a PanAnalytical Empyrean XRD instrument, operating with Cu Kα radiation in the 2θ range from 10° to 60°. We examined the morphology of the samples with a Zeiss field emission scanning electron microscope (FE-SEM), equipped with an energy dispersive X-ray spectrometer (EDS) for elemental mapping. Furthermore, surface chemical states and valence states were probed utilizing X-ray photoelectron spectroscopy (XPS). Lastly, reflectance measurements were acquired utilizing a Perkin-Elmer UV-Vis-NIR spectrometer to acquire a comprehensive characterization of the samples.

3.4 Electrochemical characterization

The performance of the catalyst towards Oxygen evolution reaction was determined in a three-electrode configuration at room temperature on an electrochemical work station. Ag/AgCl, graphite rode and casted Ni foam were used as reference, counter and working electrode respectively. Linear sweep voltammetry (LSV) was performed in 10M KOH electrolyte and also 0.5M Urea assisted electrolyte in the range of -0.5 V to 0.9 V (vs RHE) with a scan rate 5mV/S. The potential of reference electrode was converted to a reversible hydrogen electrode (RHE) by following formula:

$$E_{(RHE)} = E_{(Ag/AgCl)} + 0.59\ pH + 0.1976 \qquad (20)$$

The working electrodes were prepared by dispersing 10 mg of each Nano powder (Fe_2TiO_5 and Ru-dopped Fe_2TiO_5) in 1 ml of solution which was contain 750µl of Isopropanol, 200µl of DI and 50 µl of Nafion. The final solutions were put in in ultrasonic setup for 30 min to become uniform. After that, 70 µl of each ink was casted drop by drop in two steps (35+35) on 1cm×1cm of Ni foam which was treated by acid nitric. The Ni foams were also washed three times with DI and three times with ethanol by ultrasonic and then were put in drying oven for 24h. After that the electrochemical measurement was performed. The measurement was performed in 10 µl electrolyte also in 0.5 µl urea assisted electrolyte for both Fe_2TiO_5 and Ru-dopped sample.

4. Results and discussion

4.1 Structural Characterization

The obtained peaks in different synthesis and calcination condition (T and t) were compared to the standard peaks of pseudobrookite by taking advantage of MDI JADE 6 software and standard card of Fe_2TiO_5 (JCPDS card no 41-1432). The presence of as-synthesized compounds was also studied during the different calcination conditions. The results are shown in following graphs.

Fig.10a provides a detailed representation of the alterations in the phase composition of the powder as the annealing temperature increases in an air environment. In the X-ray diffraction (XRD) pattern associated with the sample annealed at 500-700°C for 2 hours, distinct reflections indicative of Fe_2O_3 (13.675°, 18.5, 32.80°, 40.17°, 45.37°, 49.07°) (JCPDS card no. 16-0653) are

observable. Upon further treatment at 800°C, the emergence of TiO_2 (25.42°, 31.46°, 36.64°, 37.50°, 39.41°, 41.94°, 45.40°, 49.78°, 52.29°,53.98°) in the anatase phase (JCPDS card no. 21-1236) is confirmed. Subsequent heat treatment at 900°C results in the formation of Fe_2TiO_5.

To decrease the temperature, the calcination time was extended. **Fig.10b** demonstrates that the onset of the Fe_2TiO_5 phase (2θ = 32.5°, 41.0°, 55.2°, and 62.5°) occurs at 600°C, and with further temperature escalation, the pure phase is attained. For the sample annealed at 800°C, the primary phase is identified as Fe_2TiO_5 in the orthorhombic system (JCPDS card no. 41–1432), confirmed by reflections at 2θ = 18.1°, 25.5°, 32.5°, 36.6°, 37.3°, 40.5°, 41.0°, 46.0°, 48.8°, 49.3°, 52.2°).

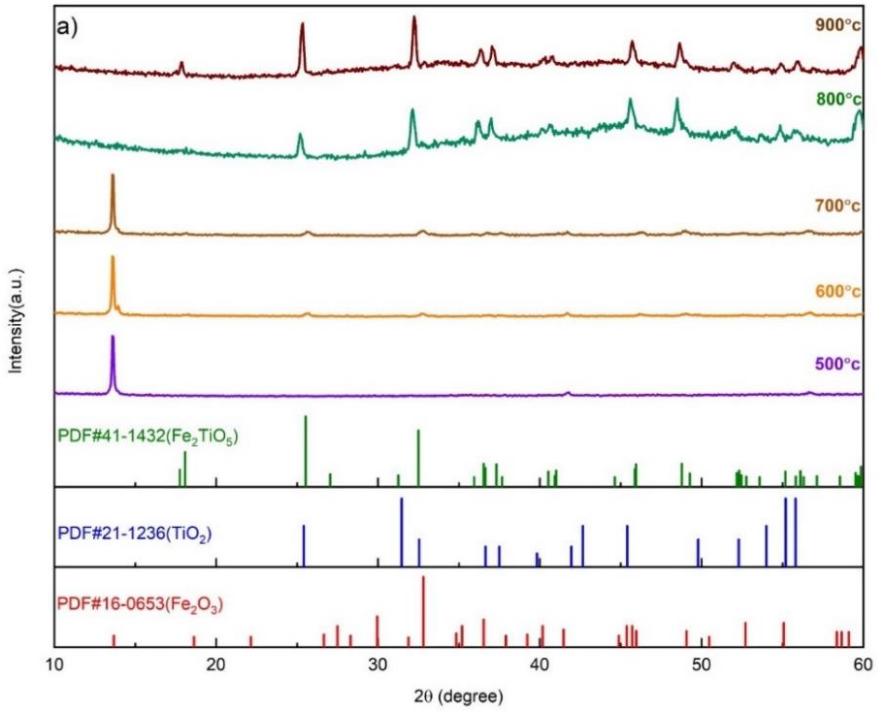

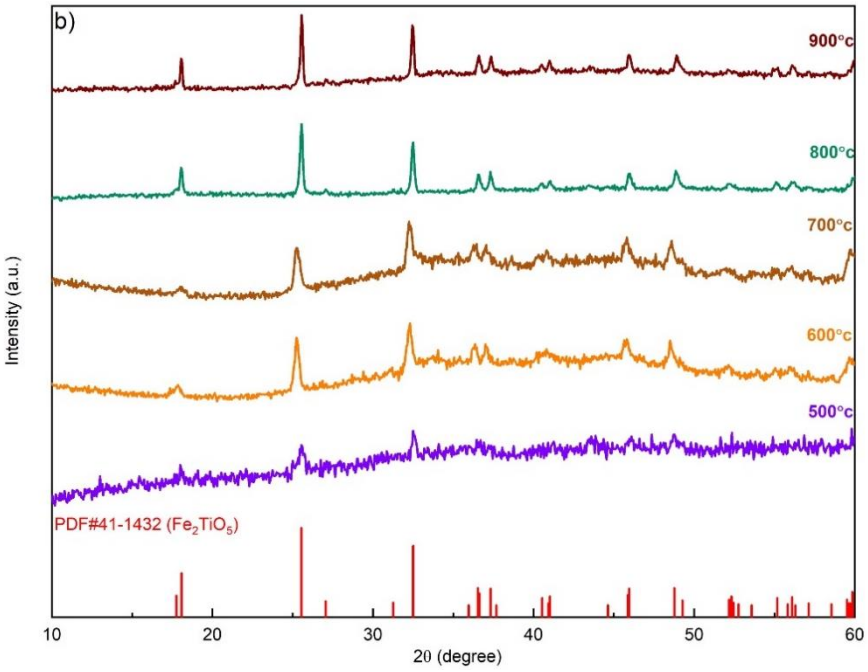

***Figure 10**: XRD patterns of the samples in* different *calcination condition time and temperature; a)2h, and b)3h*

The reproducibility of scientific procedures refers to the ability to obtain consistent and reliable results when repeating an experiment or procedure. To fulfill this the following strategy was performed. Four distinct samples were synthesized under the same synthesis conditions and calcinated at 800°C for 3h. These four samples then investigated by XRD. **Fig.11** clearly shows that the same XRD patterns were obtained for all different samples, and there is also a perfect match with the reference Fe_2TiO_5 card. The result says that the procedure is not based on try and error and resynthesis is possible.

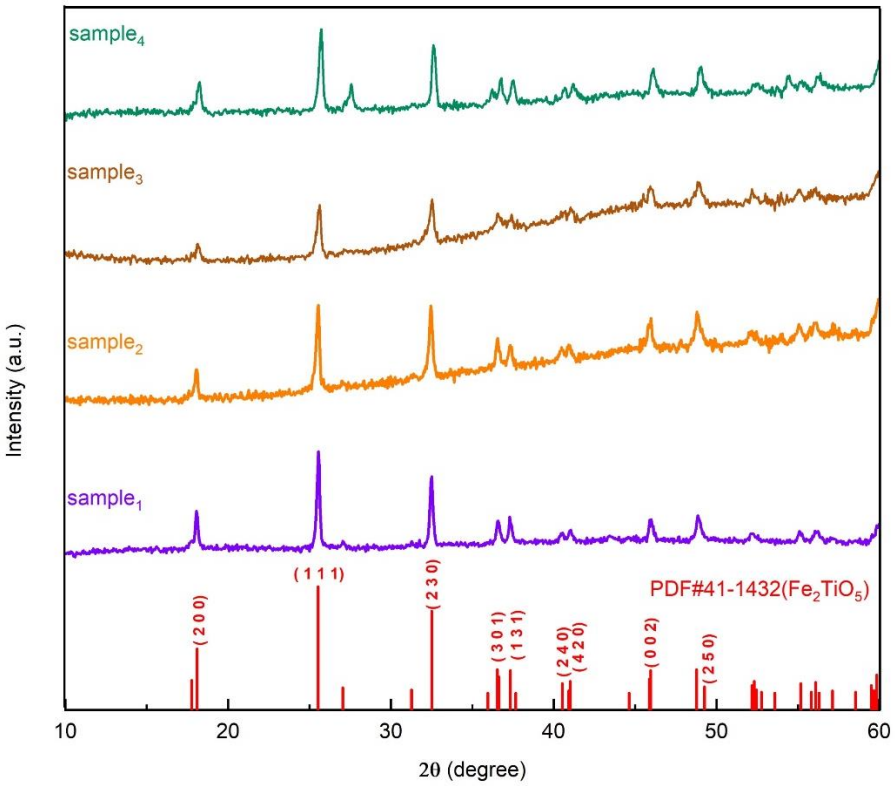

***Figure 11**. Reproducibility evidence for different samples*

Next, we looked into the doping accuracy and its effect on the crystal structure of our sample. Evaluation of doing process was done by comparing the peaks of the Ru-dopped Fe_2TiO_5 by the reference peaks of the most probable compounds. The following strategies were done in this step. Initially, three samples were prepared using the methods listed below:

S1) $RuCl_3$ + Fe_2TiO_5 with the ratio: 1:2 then calcination in 400°c for 3h (without Hydrothermal)

S2) $RuCl_3$ + Fe_2TiO_5 with the ratio: 1:1 then calcination in 400°c for 3h (with Hydrothermal)

S3) Reagents of pseudobrookite + $RuCl_3$ then calcination in 800°c for 3h

As illustrated in **Fig.12**, all the methods mentioned were rejected due to the formation of RuO_2, which was not our desire.

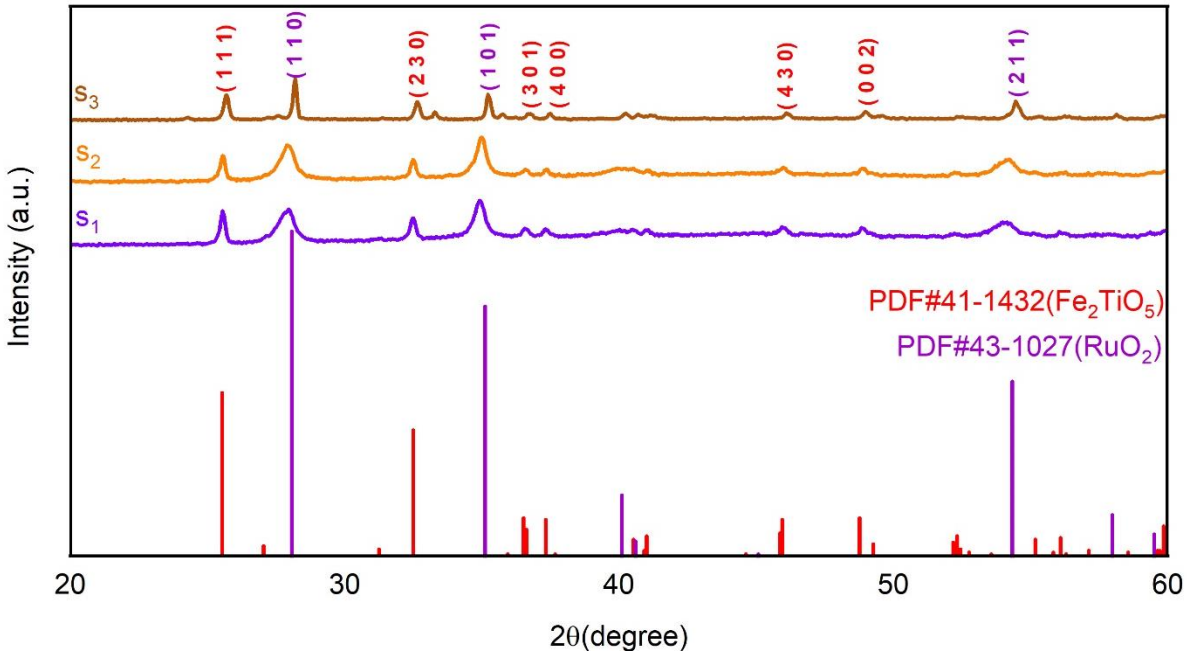

***Figure 12**. XRD patterns of Ru-doped samples through 3 different doping strategies*

Based on the reason mentioned above, another procedure was chosen. In this method Ar calcination was used instead of normal calcination. In this procedure 0.12gr of Fe_2TiO_5 with 0.04 gr of $RuCl_3$ dissolved in ethanol and DI based on the procedure and final calcination was carried out in the presence of Ar in CVD setup. The final powder was investigated by XRD and the result is shown in **Fig.13**.

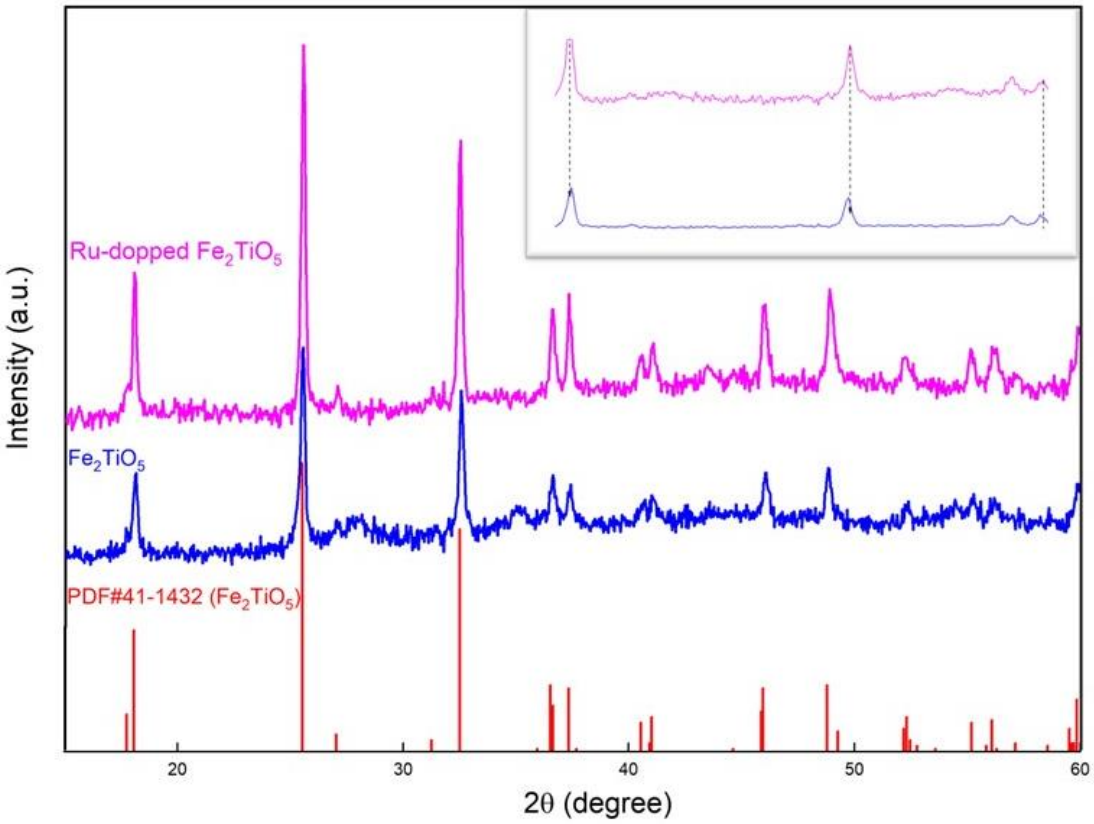

***Figure 13**. XRD patterns of Ru-doped sample calcinated in Ar*

As it can be concluded from the **Fig.13** after doing the calcination in Ar atmosphere the oxide as-products were completely removed and a clear shift in the peaks were observed (forward shift). We can interpret this result like this. When a chemical undergoes calcination in Oxygen it means that the pure Oxygen is present and due to the fact that Oxygen is highly reactive the first thing which is expected is the facilitation of the combustion that leads to the formation of oxide products. In contrast, Ar is chemically inert and does not readily participate in chemical reactions. Therefore, calcination in Ar can be advantageous in certain cases where the presence of Oxygen could lead to unwanted reactions or oxidation of the material being calcined. An atmosphere of argon can be used to provide a controlled environment with low chemical reactivity during the calcination process. This can be especially helpful when calcining materials that are oxidation-sensitive or that need certain circumstances to retain their desirable characteristics.

4.2 Morphology characterization

The SEM technique was used to explore the surface morphology of the samples heat-treated at 800 ◦C at 3hr in air. As can be seen from **Fig.14**, samples had the confirms the dense structure with the formation of rounded particles with sizes 500 nm particles without agglomeration.

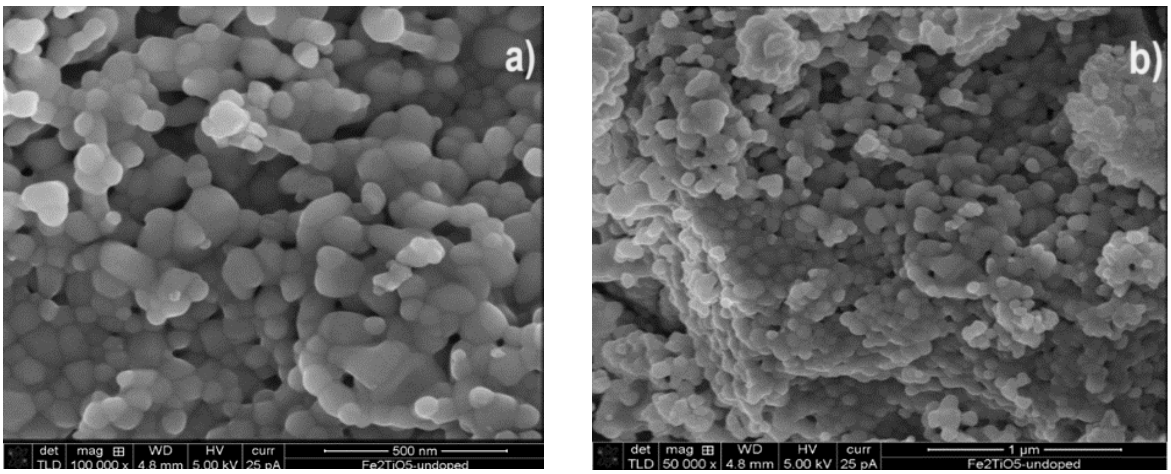

***Figure 14**. SEM micrographs of pseudobrookite*

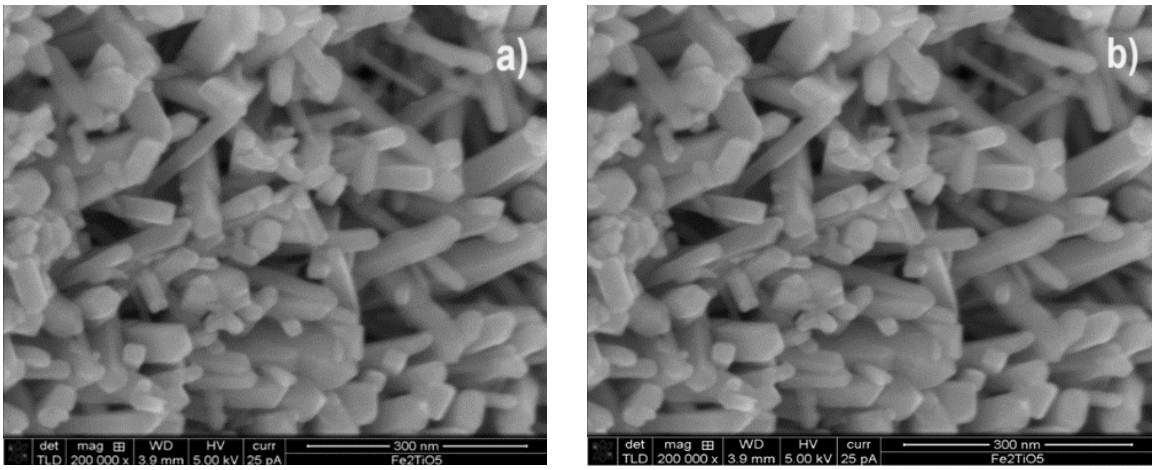

***Figure 15**. SEM micrographs of Ru-dopped pseudobrookite*

The micrographs in **Fig.15** demonstrate the impact of Ru's doping. The majority of the particles' morphology was spherical prior to doping, but after doping, this all altered, giving us a one-dimensional structure.

Morphological design and fabrication of nanostructured electrocatalysts has an important effect on the efficiency of water splitting system and provide significant benefits for their performance. One-

dimensional (1D) nanoscale materials have been shown to be a unique target among many morphologies and architectures for providing strong electrocatalyst candidates. Firstly, the huge surface areas, large roughness factors, and high active-site densities of these 1D materials are advantageous in terms of effectively supplying catalytic activity for surface electrochemical reactions. Second, quick charge transport paths with less dispersion can be made possible by the channels and few crystal barriers that 1D materials can offer. Third, the presence of copious free space and porosity between neighboring 1D nanostructures allows electrolyte molecules to be chemically accessible and transported quickly into the deep area of the electrode/catalyst surface. Fourth, the 1D materials can be instantly grown and contacted on the underlying electrode surface, and consequently give efficient charge transport with low contact resistance, as well as eliminate the need of adding conducting additives or binders. Fifth, the surface of the 1D nanomaterial electrode/catalyst can also aid in the production and release of bubbles, preventing the bubbles from obstructing the succeeding reaction process [45].

Based on all the reasons which are mentioned above, it can be concluded that doping by Ru has also positive effect on the catalyst performance by tailoring the morphology and formation a one-dimensional structure.

4.3 Energy Dispersive X-ray characterization

The following micrographs **(Fig.16-21)** for Fe_2TiO_5 and Ru-dopped sample were obtained using energy dispersive X-ray spectrometer (EDS)

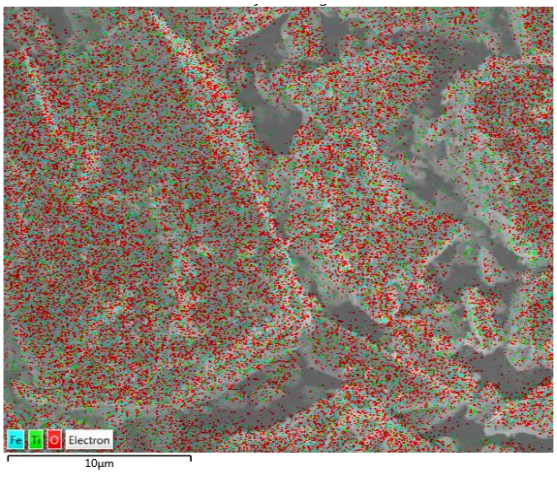

***Figure 16**. Elemental mapping of pseudobrookite*

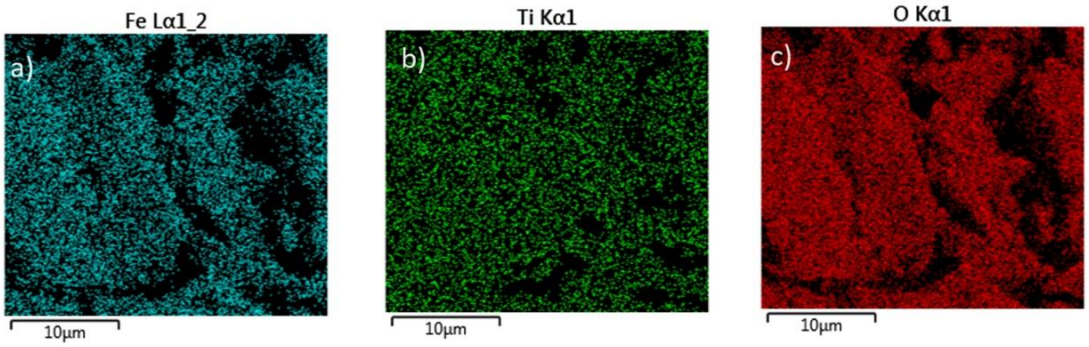

***Figure 17**. Elemental mapping of (a) Iron, (b) Titanium, (c) Oxygen of pseudobrookite*

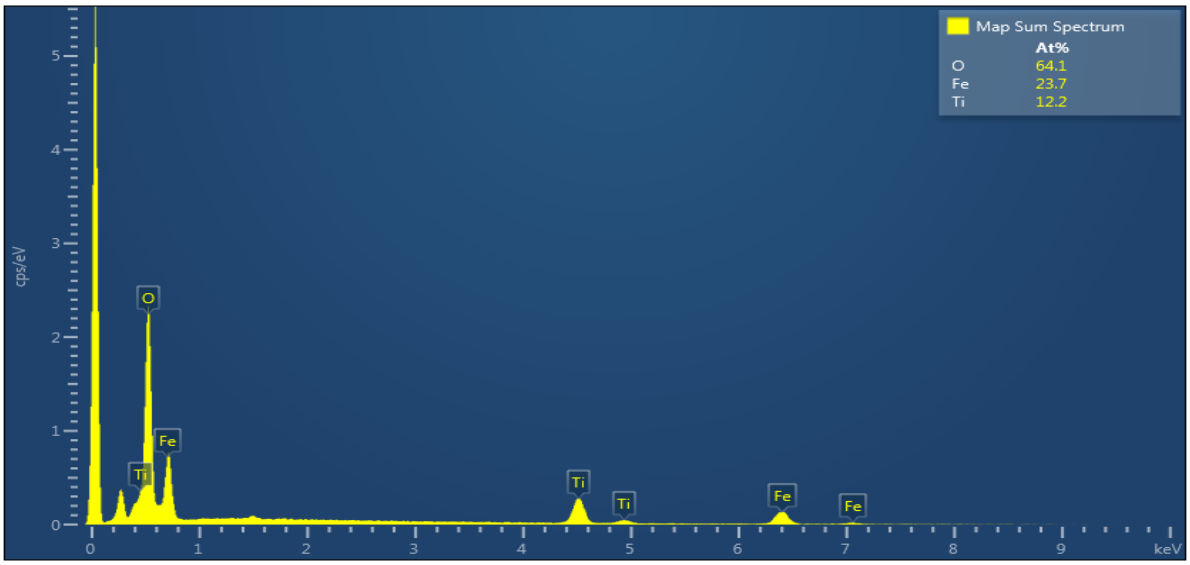

***Figure 18**.EDS graph of pseudobrookite*

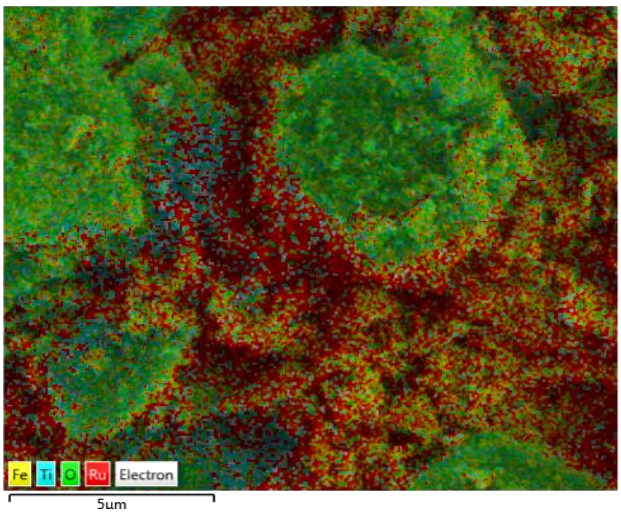

***Figure 19**. Elemental mapping of Ru-dopped pseudobrookite*

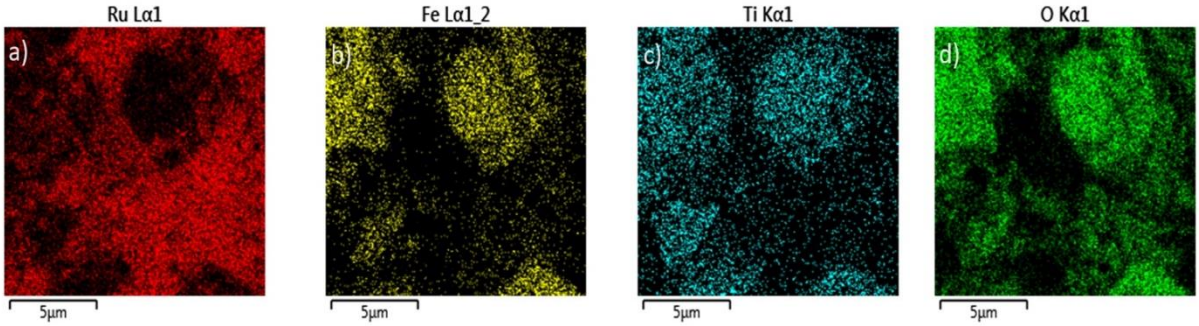

***Figure 20**. Elemental mapping of(a) Ru, (b) Iron, (c) Titanium, (d) Oxygen*

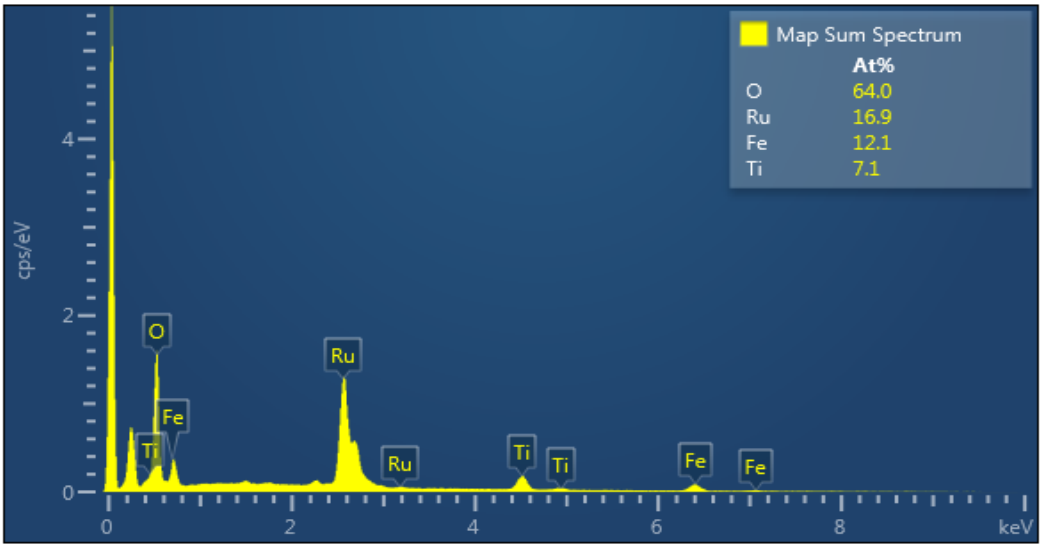

***Figure 21**.EDS graph of Ru-dopped pseudobrookite*

From EDX analysis, the presence of Iron, Titanium, Oxygen and Ruthenium was detected, as confirmed by the EDX mapping in **Fig.18** and **21** as well. The main signals (Ru, Fe and Ti) are coming from the precursors which were used during synthesis procedure. On the contrary, the signals coming from Oxygen can be related also to the precursors as well as an imperfect washing process after centrifuge since DI should eliminate the presence of such impurities. As an alternative to explain the presence of Oxygen, also the following hypothesis are valid like adsorption of Oxygen at the surface and partial surface Oxidation. Therefore, these factors can be considered to justify the presence of a signal coming from Oxygen. On the other hand, **Fig.16** and **19** make it possible to observe the presence of Iron, Titanium and Ruthenium on the surface. So, it can be claimed that the doping process affects the surface, morphology and the structure of nanomaterial.

4.4 Optical Characterizations

Although our aim of producing this material was to use it as an electrocatalyst, the optical properties of Ru-dopped sample was investigated through a UV-Visible spectrophotometer in reflectance mode to determine its efficiency also as a photocatalyst. In **Fig.22** the optical resistance spectra for Ru-dopped sample under investigation is reported.

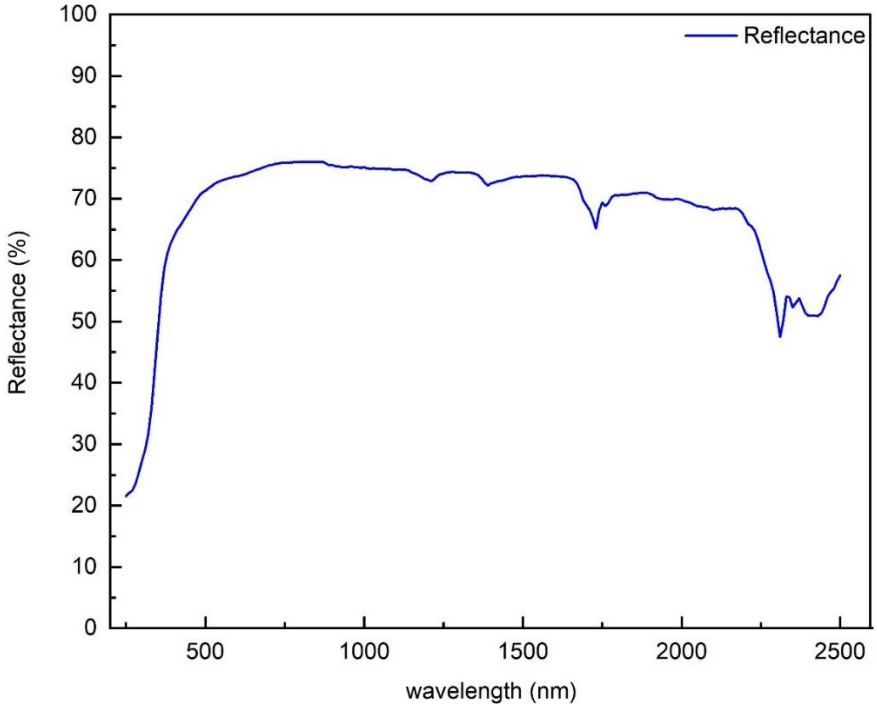

***Figure 22**. optical reflectance spectrum of Ru-dopped Fe_2TiO_5*

By taking advantage of Kubelka and Munk equation following graph can be obtained.

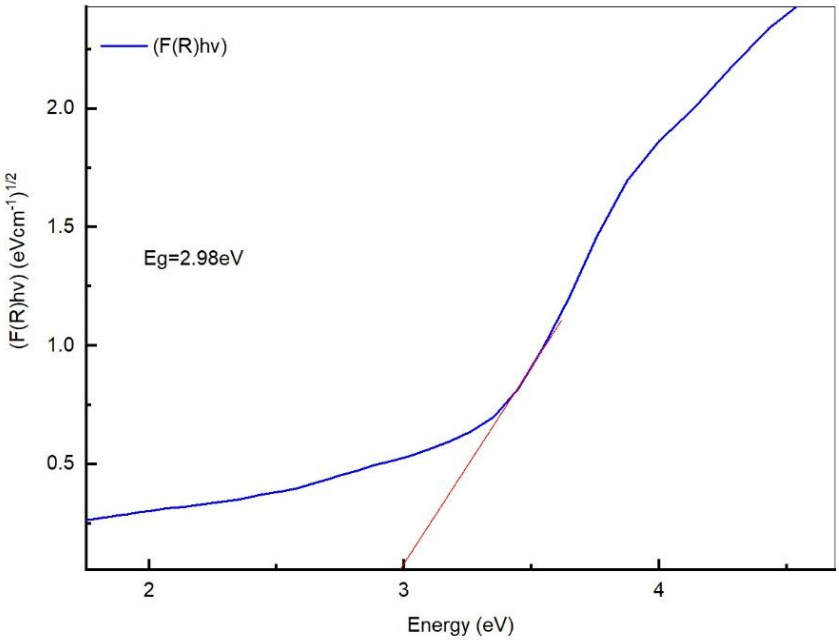

***Figure 23**. Tauc plot of Ru-dopped Fe_2TiO_5*

It can be observed that Ru-dopped sample shows an acceptable ability to use also as a photocatalyst. due to the fact that the Ru-dopped sample with a 2.98 eV bandgap energy has the basic conditions for use as a photocatalyst. These conditions include having the energy of bandgap greater than 2 eV and also a minimum value 1.23 eV which is the lowest potential for water splitting [46].

4.5 Photoelectron spectroscopy characterization

The XPS protocol presented here was used to study the change in surface composition and electronic structure of the elements which are present as a result of Ru doping. As mentioned before, the key factor in electro chemical reactions is the electron transfer and any change in electronic structure leads to the change in gain-loss electron behavior. The assessment of surface chemical states and valence states of Fe, Ti, O, and Ru in Fe_2TiO_5 and Ru-doped Fe_2TiO_5 was conducted using X-ray photoelectron spectroscopy (XPS). **Fig.24 and Fig.25** present a wide range of spectra for both doped and undoped samples, confirming the presence of Ru, Fe, Ti, and Oxygen elements at their respective binding energies. To further investigate electronic structure changes, narrow-scan spectra for each element were measured.

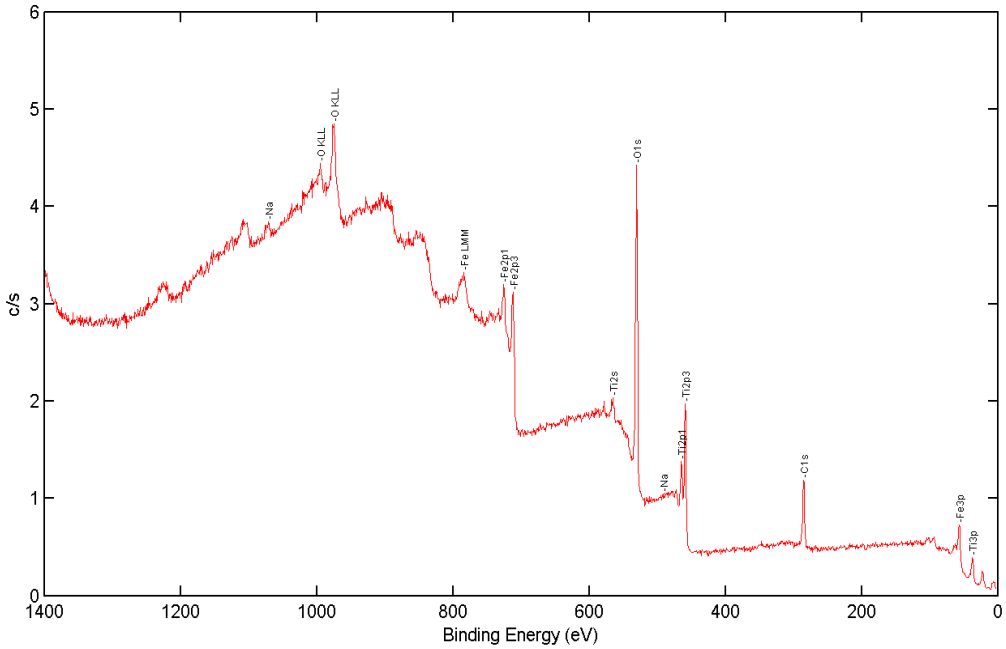

***Figure 24**. Overview spectrum of Fe_2TiO_5*

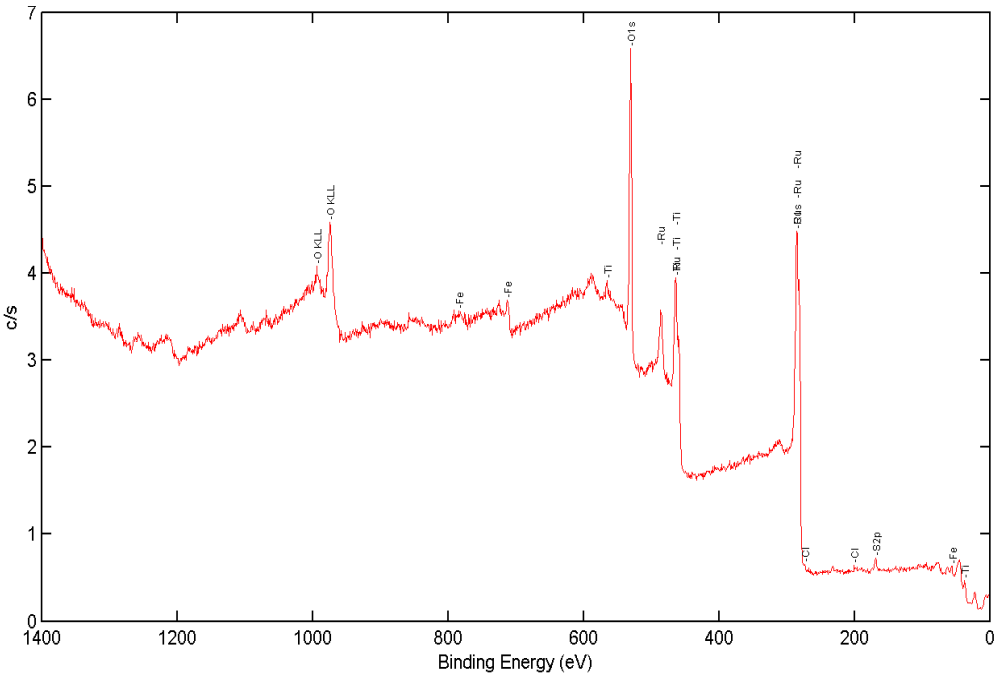

***Figure 25**. Overview spectrum of Ru-dopped Fe_2TiO_5*

The Ti 2p binding energies observed in Fe_2TiO_5 are approximately 458.3 eV and 463.9 eV, indicating Ti^{4+} oxidation states as illustrated in **Fig.26a.** In the case of Ru-doped Fe_2TiO_5, the Ti 2p3/2 binding energy at 458.7 eV reveals a shift to higher binding energy, specifically by 0.4 eV. This shift serves as confirmation of the oxidation of Ti during the Ru doping process. However, the doublet Ti 2p1/2 is obscured by the Ru 3p3/2 signal, as depicted in **Fig. 26b**. To further validate the Ti (IV) oxidation state, we examined the Ti 3p spectrum (**Fig.27c**). The Ti 3p spectrum confirms the presence of Ti (IV) ions, which are octahedrally coordinated by oxygen ions.

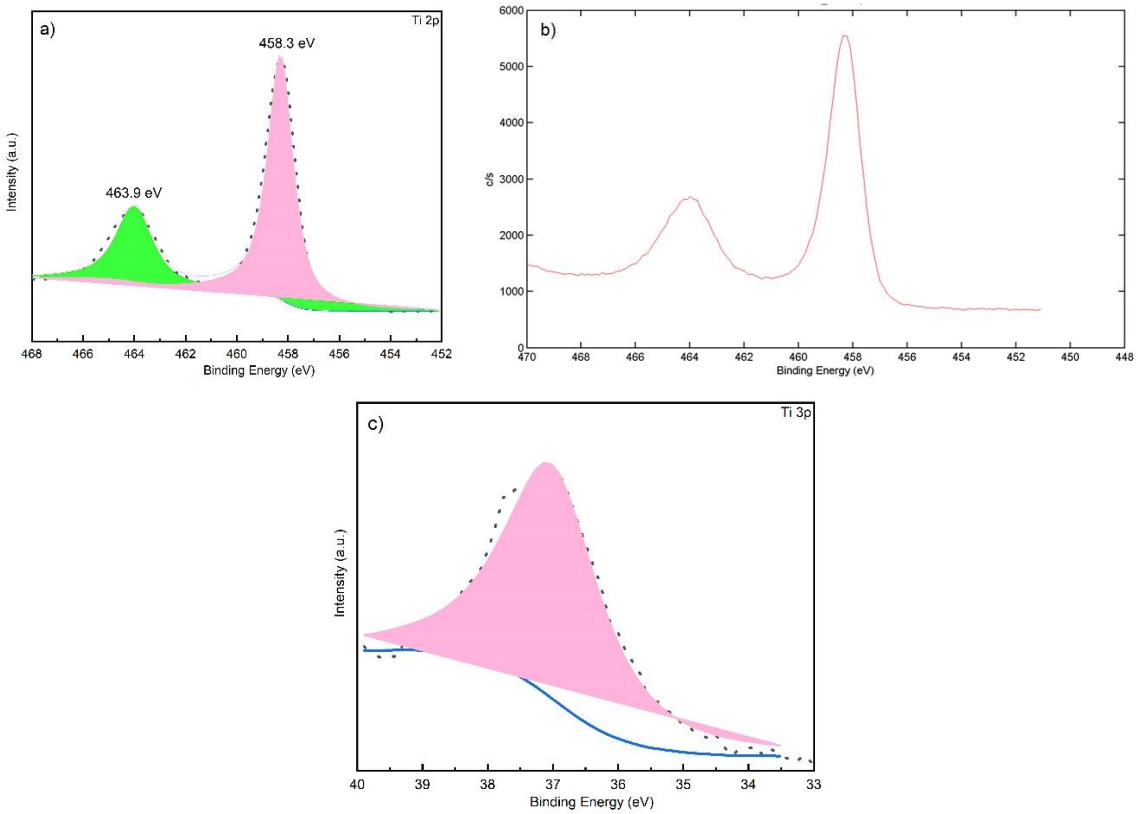

Figure 26. *High-resolution spectra of a) Ti 2p,b) Overview spectrum of Ti 2p1/2in Ru-doped Fe_2TiO_5 and c) High-resolution spectra of Ti 3p*

The Ru 3d peaks observed at 282.1 eV and 286.0 eV in **Fig.27a** provide confirmation of Ru^{4+} oxidation states. However, due to signal overlap with C 1s, we measured the Ru 3p1/2 peak at 488.1 eV, which further substantiates the presence of Ru^{4+} in Ru-doped Fe_2TiO_5. Nevertheless, additional peaks at 484.7 eV (**Fig.27b**) in both Ru 3d and Ru 3p spectra, along with a peak at 280.5 eV, indicate the presence of unreacted Ru (0) on the surface.

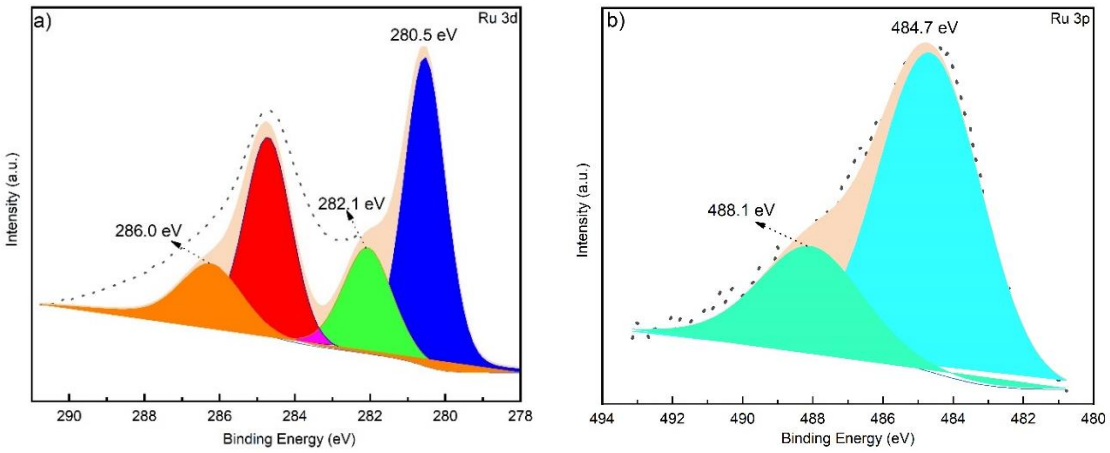

***Fiureg 27**. High-resolution spectra of a) Ru 3d and b) Ru 3p*

The XPS O 1s spectrum (**Fig.28**) was deconvoluted into two peaks at 529.9 eV which is associated with lattice oxygen and another peak at around 531.4 eV was attributed to chemisorbed oxygen (Fe-OH), respectively.

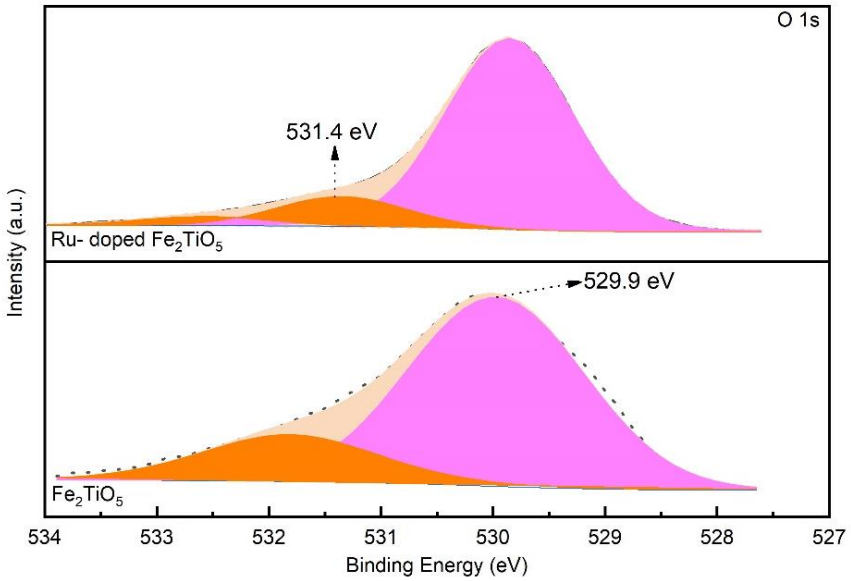

***Figure 28**. High-resolution spectra of O 1s*

In the Fe 2p spectrum of Fe_2TiO_5 (**Fig.29a**), contributions at 724.1 eV and 710.8 eV corresponded to Fe 2p1/2 and Fe 2p3/2, respectively, indicating Fe^{3+} with a 13.3 eV gap. Deconvolution revealed a contribution at 713.4 eV, and satellite peaks at 719.1 eV and 732.7 eV confirmed the oxidation state of Fe^{3+}. In Ru-doped Fe_2TiO_5, Fe 2p spectrum (**Fig.29b**) showed similar peaks, with a slight

shift of 0.2 eV towards lower binding energies, suggesting electron density redistribution between Ru and Fe in the surface region.

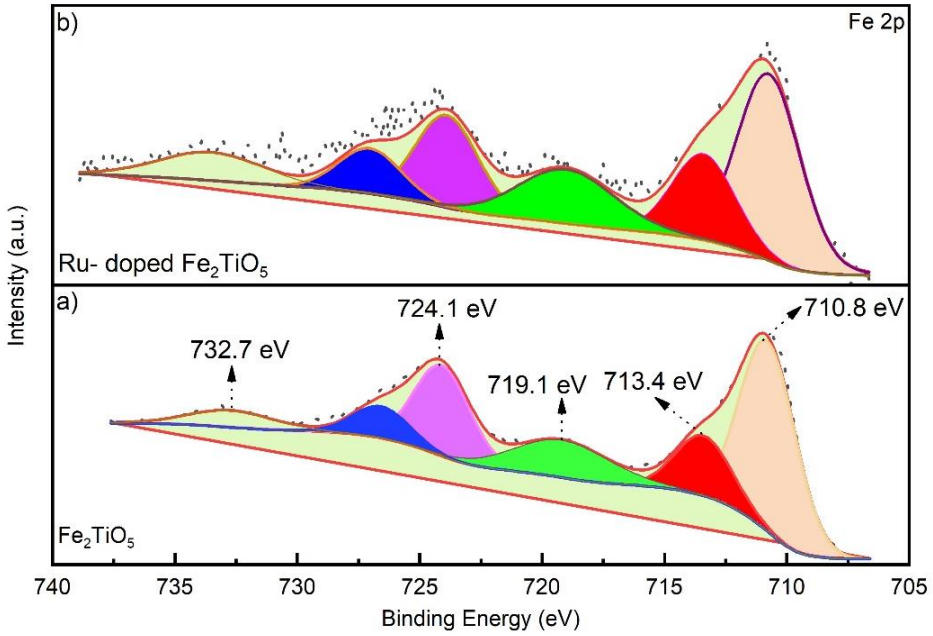

***Figure 29**. High-resolution spectra of a) Fe 2p of Fe_2TiO_5 and b) Ru-doped Fe_2TiO_5*

4.6 Electro chemical measurements

The electrocatalytic performance of bare sample and Ru-dopped one for OER was firstly evaluated by LSV. **Fig.30** shows the LSV curves of Fe_2TiO_5 and dopped sample in KOH and urea assisted electrolytes.

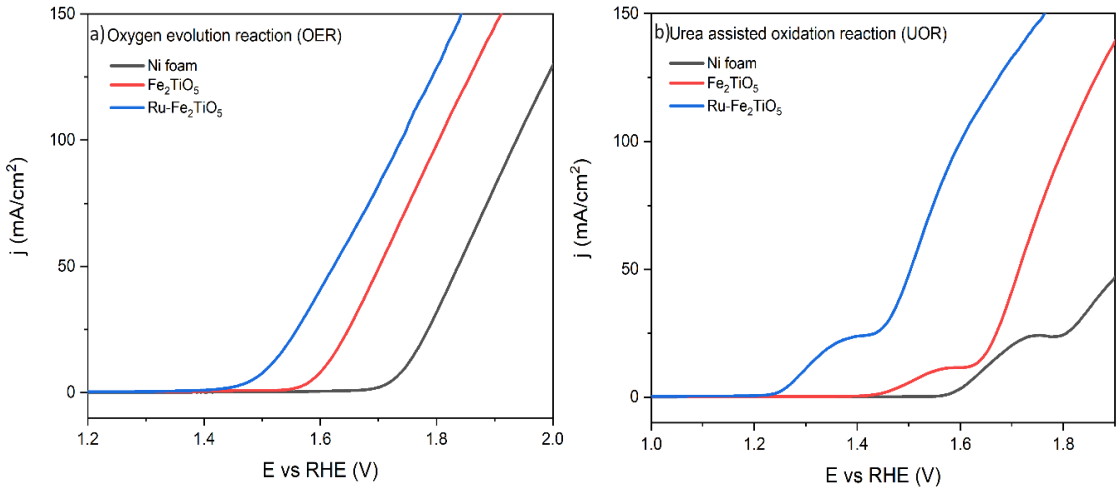

***Figure 30**. Linear sweep voltammetry for Fe_2TiO_5 and Ru- dopped Fe_2TiO_5 in a) Oxygen evolution reaction and b) urea assisted Oxidation reaction*

Using the obtained results, the enhancement and strengthening of the catalytic activity can be explained in two aspects; doping by Ru and taking advantage of Urea to assist Oxidation reaction. The Ru-dopped electrocatalyst exhibits enhanced performance compared to bare Fe_2TiO_5. The current density of $10mAcm^{-2}$ is the operation current of electrocatalysts, and the working voltage under this value is important to evaluate the performance for OER electrocatalyst. As shown in **Fig.30a** the Ni foam exhibits poor activity towards the OER with the 490 mV in overpotential. This value is 350 mV for Fe_2TiO_5 but after doping by a small amount of Ru, the Ru-dopped Fe_2TiO_5 exhibits an improved catalytic performance requiring an over potential of 230 mV to achieve a current density of 10 $mAcm^{-2}$.

In the next step the effect of adding small amount of Urea to assist the Oxidation reaction was evaluated. To do this, the LSV measurement was performed for three other samples in the same condition but in 0.1M Urea assisted electrolyte. The results are shown in following table.

Material	Onset potential OER (V)	Onset potential UOR (V)	Overpotential OER (mV)	Overpotential UOR (mV)
Ni foam	1.72	1.58	490	350
Fe_2TiO_5	1.58	1.56	350	330
Ru-dopped Fe_2TiO_5	1.46	1.38	230	150

***Table1**. comparative list of experimental data of onset and overpotential in OER and UOR*

As it can be seen there is clear drop in onset and overpotential for all three samples in Urea-assisted electrolyte compare to non-assisted one. The obtained values for overpotential are 350, 330 and 150 mV for Ni foam, Fe_2TiO_5 and Ru-dopped Fe_2TiO_5 respectively, while these values were 490, 350 and 230 mV in OER. Among all the results, the lowest value in overpotential is related to Ru-dopped Fe_2TiO_5 in Urea-assisted electrolyte. By comparison between the overpotential of Ru-dopped Fe_2TiO_5 in UOR (150mV) and Ru-dopped Fe_2TiO_5 in OER (230mV) it can be concluded that adding just a little amount of Urea leads to a 34.78% drop and consequently the enhancement of photocatalytic performance. Following graph provides a complete overview about the effect of doping and assistance of electrolyte by adding Urea.

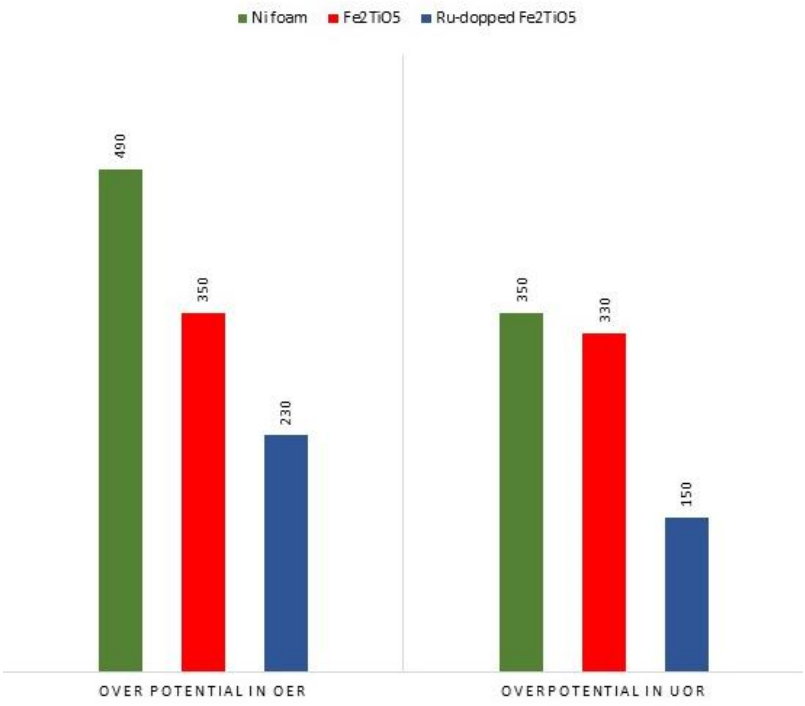

***Graph1**. comparative list of experimental data overpotential in OER and UOR*

Eventually, this drop in overpotential can be justified due to the fact the presence of 4 hydrogen bonds between the hydrogen and Nitrogen in the chemical structure of Urea. The bond energy of H-N in these hydrogen bonds is much lower than the O-H due to the higher electronegativity of Oxygen compared to Nitrogen. Therefore, much smaller amount of energy is required to break these bonds and consequently lower required energy for Oxidation reaction. It can be said that by taking advantage of both doping by Ru and assistance of electrolyte medium by adding a small amount of Urea an enhancement of electrocatalytic activity can be achieved.

As mentioned before, the Tafel plot is an important parameter for evaluating catalytic kinetics. To farther analyze the electro catalytic activity of our catalyst, Tafel plot of the bare Fe_2TiO_5 and Ru-dopped Fe_2TiO_5 were derived from LSV curves by fitting the linear regions according to the Tafel equation. The corresponding results are shown in **Fig.31**.

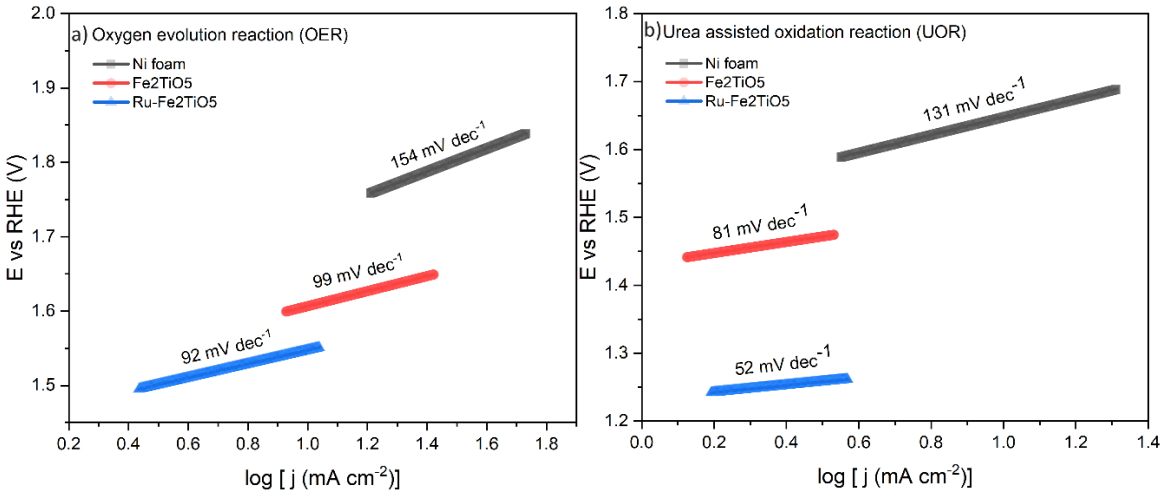

***Figure 31**. The Tafel plots of Fe_2TiO_5 and Ru- dopped Fe_2TiO_5 in a) Oxygen evolution reaction and b) urea assisted Oxidation reaction*

It can be observed that the Ru-dopped Fe_2TiO_5 shows a Tafel slop 92 mV dec^{-1}, lower than that of bare one 99 mV dec^{-1} in OER. This value is 52 and 81mV dec^{-1} in Urea assisted electrolyte respectively. The Tafel plot generally illustrates a linear relationship between the overpotential and the current logarithm. The Tafel slope, which is correlated with the reaction's activation energy, is shown by the slope of the curve. Consequently, the reaction rate is demonstrated by the slope. The kinetics is slower and larger activation energy is required for the reaction to occur on steeper slopes. These results indicate that Ru-dopped sample in Urea assisted electrolyte with the lowest Tafel slop possesses a higher kinetics towards Oxidation reaction compare to bare sample and alkaline electrolyte. The reason for this result can be attributed to the following possibilities. At first, we have the expanding the active sites as a result of doping by Ru. Secondly, the presence of Ru leads to the tuning of energy levels and modification of energy levels consequently leads to a better match in the energy requirements of water splitting reaction. This alignment of energy level enables easier electron transfer. And finally, Ru doping enhances the electron mobility by modifying the conductivity of electrocatalyst and consequently electron movement.

An essential component in the designing of electrocatalysts is stability. After evaluation of the Ru doping as a practical way to enhance the catalytic activity, we focused on the durability of our catalyst. There are different methods to measure the stability of a catalyst. Herein the practical operation of the catalyst was examined by electrolysis at fixed current densities (10,50 and 150 $mAcm^{-2}$) over extended periods (36h). The result is shown in **Fig.32.**

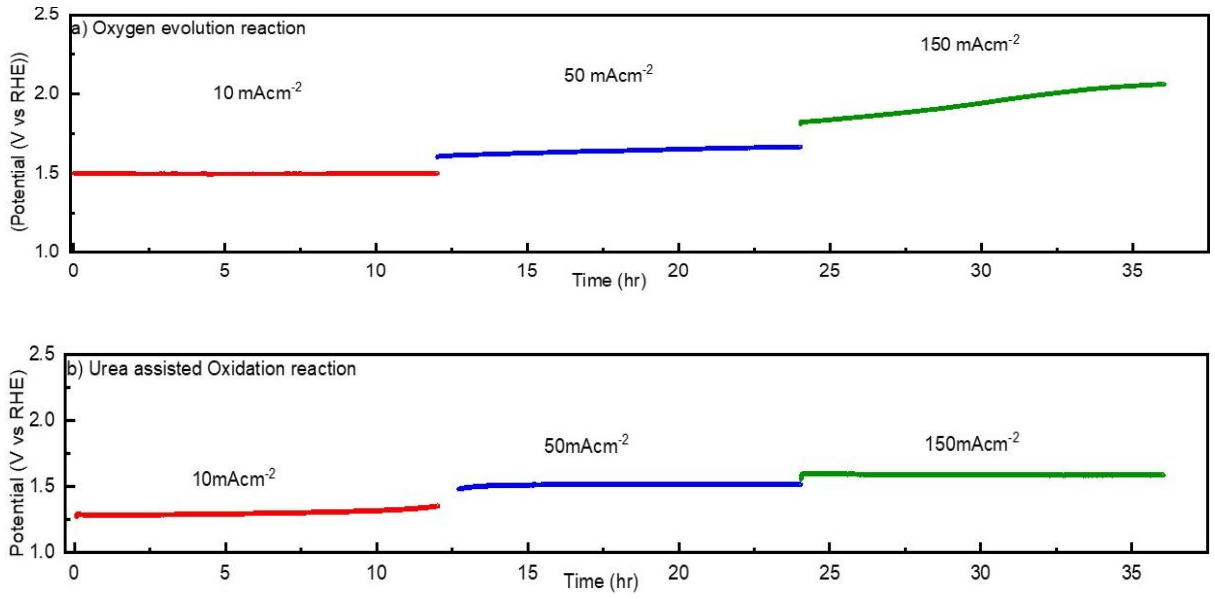

***Figure 32**. Time dependence of overpotential during electrolysis over 36 h at fixed current densities in a) OER and b) UOR of Ru-doped Fe_2TiO_5*

At a lower current density of 10 and 50 macm^{-2}, the catalyst potential remains stable at ~1.5V in OER and 1V in UOR for electrolysis over 36h. At higher current density (150 mAcm^{-2}) a little increase in potential of less than 10% was observed only in OER, this change in potential was not seen in Urea-assisted Oxidation reaction. It is important to mention that the increase in potential of the sample in OER was observed during last several hours and the potential was almost fixed during first hours. This remarkable resilience indicates potential for long-term useful applications of the catalysts.

5. Conclusion

One of the most promising energy portfolio strategies for the future is electrocatalytic water splitting, which produces pure H_2 when powered by renewable energy sources. However, due to thermodynamics barrier and being an uphill chemical reaction, the presence of the catalysts to overcome kinetic obstacle is an essential.

This thesis provides a simple and facile approach to synthesis Ru-dopped Fe_2TiO_5 electrocatalyst through a protocol that has not been reported in literature yet. The protocol consists of two steps: a) Fe_2TiO_5 synthesis and b) doping process by Ru. In the first step, pseudobrookite Nanoparticle has been obtained by a facile synthesis involving iron nitrate and titanium isopropoxide as metal precursors. The strategy for the synthesis of Fe_2TiO_5 was justified by XRD characterization and finding a perfect match between the XRD peaks of the sample which was calcinated at 800^{o} C for 3h and the reference peaks of Fe_2TiO_5 (PDF#41-1432). In the second step, the doping was done to enhance the catalytic activity of bare pseudobrookite for water splitting application.

The doping protocol also was confirmed by observing a forward shift in the XRD peaks of the sample which was calcinated in Ar at 300°C for 2h compared to the peaks of bare sample. Regarding to synthesis strategy and further doping the presence and distribution of the elements was also confirmed by EDX characterization and elemental mapping of the bare and Ru-dopped sample. The morphological effect of the doping was evaluated by scanning electron microscopy. SEM micrographs shows a changing of morphology of bare Fe_2TiO_5 Nano powder from 0D to 1D. 1D morphology is a well-known and excellent morphology in the field of electrocatalyst. This aim was obtained after doping due to the presence of Ru atoms. Although our focus was on the application of this material in the field of electrocatalyst, we also evaluate its performance as photocatalyst. To do this, we performed the UV-VIS measurement and by using Tauc equation we obtained the energy of the band gap for this material which was 2.98 eV that is a suitable value also for photocatalysts. The surface electronic states of the developed catalysts were analyzed by X-ray photoelectron spectroscopy (XPS). The high-resolution XPS survey scan spectra of Fe2TiO5 and Ru-dopped sample were obtained. The high-resolution spectra of the elements were also obtained to determine the electronic state of the elements before and after doping and changing in electronic structure of the elements was observed by changing in binding energy value (0.2 eV towards lower binding energies for Fe 2p spectrum after doping).

Electrochemical measurement with a three-electrode configuration were led through potentiostatic analysis which made it possible to study the performance of this material for OER. Ru-dopped material has been demonstrated to have remarkable efficiency in Oxygen evolution reaction compared to bare sample. In this step we took advantage of Urea to enhance and improve the Oxygen reaction rate and this led to obtaining the lowest overpotential value (150mV) for the Ru-dopped sample in Urea assisted electrolyte compared to all other samples. This result was also confirmed by the study the Tafel plot slop and the highest kinetics value was related to Ru-dopped sample in UOR, having the lowest Tafel plot slop (52 mV dec^{-1}).

The outstanding result was also obtained during stability test. The data shown just a negligible increase in over potential only for non-assisted electrolyte during 36h. These allow to conclude that Ru doping in Urea assisted electrolyte can effectively adjust the composition and reaction and hence improving the electrocatalytic activity of Oxygen evolution reaction.

Based on the above reported results and discussions, the enhanced performance in Oxidation reaction can be ascribed to the following two aspects: a) Ru doping in that made the compound even more electron rich and this guaranteed a higher conductivity, surface activity and more active catalytic sites. b) taking advantage of Urea as an excellent approach to promote the charge transfer at the interface between the electrodes and electrolyte due to its easier chemical decomposition and faster charge carrier mobility.

To learn more about the characteristics and the factors that may be adjusted to create catalysts that are even more effective, extra characterization techniques in the field of electrochemical measurement could be helpful. An approach would be calculation of faradic efficiency to guarantee that the Oxidation current generates from the release of Oxygen rather than other side reactions. Also, electrochemically active surface area and electrochemical impedance spectroscopy (EIS) to further investigation of Oxidation reaction between bare and dopped samples in both alkaline and Urea-assisted electrolyte.

Our approach provides a new idea for the catalyst design and creates new opportunities for advancing clean energy systems based on Ru-dopped electrocatalyst. This product could be produced at a larger scale by using more affordable and plentiful composite nanostructures in place of traditional noble-metal catalysts because of its simple synthesis process and quick kinetics in Oxidation reaction.

6. Appendix

6.1 Structural, morphological and optical characterization

6.1.1 X-Ray diffraction

Our knowledge of the atomic structure of solids has been completely transformed by X-ray diffraction, which also yields vital information about the physical and chemical characteristics of a variety of materials. By analyzing the interference pattern that results from a plane wave interacting with itself after passing through a series of small, spaced apertures, researchers can precisely investigate the ordered arrangement of atoms in solids. The X-ray diffractometer works on the fundamental principle of utilizing electromagnetic radiation's interaction with crystalline solids through the process of constructive and destructive interference. Alternating bright and dark spots that represent areas where the generated waves are either in phase or out of phase, respectively, define the resulting pattern. When X-rays interact with the electrons that surround atomic nuclei, they scatter in all directions, creating spherical wavefronts. Laue's conditions are met when these wavefronts meet, causing constructive interference and increased intensity, as seen in **Fig.33**. This makes it possible to precisely and accurately analyze the atomic structure of solids, giving scientists important new information about the chemical and physical characteristics of these materials.

By examining the X-ray diffraction pattern and the angle of the diffraction peaks, researchers can gather vital information on the crystal lattice of various materials. give details about the atoms' spacing and symmetry within the crystal lattice, but the peak intensities provide details about the distribution of electron density inside the crystal. Researchers can ascertain a material's crystal structure, including its crystal symmetry and unit cell characteristics, by examining these peaks. Other significant characteristics of materials, such as their preferred orientation and texture, can also be seen in the diffraction pattern. Because of the wide-ranging implications these discoveries about the structure and characteristics of materials have for physics, chemistry, geology, and materials science, the X-ray diffractometer has become a vital tool in the field, helping researchers gain a deeper understanding of the atomic structure and behavior of materials. Numerous technological developments and improvements in the design and performance of materials have resulted from the insights and advancements that followed.

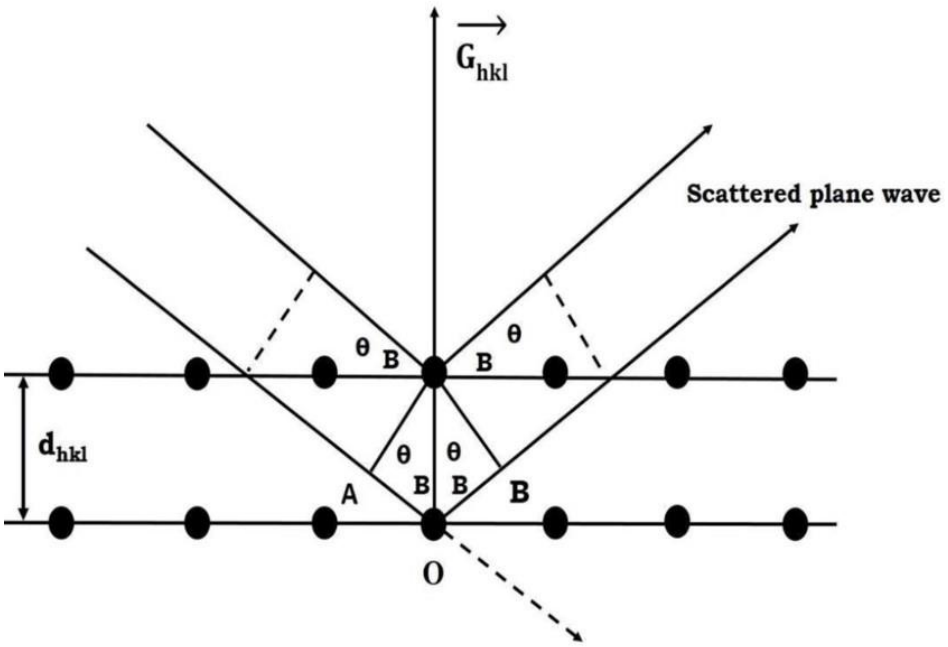

Figure 33. *schematic representation of scattered waves.*

Another way to express the constructive interference is the Bragg's law, which read as follows:

$$2d_{hkl}\sin\theta = n\lambda \qquad (21)$$

The variables θ, λ, and dhkl indicate the incident angle, wavelength, and interplanar distance, respectively, between the plane given by miller indexes and the material surface, where n is an integer number between 0 and infinite. Bragg's law states that only if the wavelength of the X-rays is an integer multiple of the spacing between adjacent planes of atoms in the crystal lattice will the incident radiation, when directed at the proper angle, diffract in a way that results in constructive interference. Put another way, if the path difference between the diffracted beams is equal to an integer number of wavelengths, then the beams will be in phase and cause constructive interference.

In other words, we can identify families of planes in the crystal lattice that contribute to the constructive interference of X-rays by varying the angle 2θ, which in this case is the angle between the incident and diffracted X-rays. This information can be used to determine the atomic structure of the crystal and the positions of the atoms in the crystal lattice.

A high voltage supply is usually part of the XRD setup, which produces X-rays from a copper anode. After that, the concentrated X-ray beam is run via a monochromator, which determines which X-ray wavelength will be utilized in the investigation. After this monochromatized beam interacts with the sample, a detector placed within a preset angle range records the resulting diffraction pattern.

A diffraction pattern that can be utilized to determine the sample's composition and crystal structure is produced by varying the X-rays' angle of incidence throughout a range of angles. After that, the diffraction pattern is examined with specialized software and libraries to ascertain the locations and diffracted peak intensities.

One of the key advantages of XRD is that it is a non-destructive technique, meaning that it does not require the destruction of the sample to obtain the necessary data. This is particularly important for samples that are rare, precious, or otherwise difficult to obtain. In addition, XRD can be used to analyze very small amounts of material, if the sample possesses a well-defined crystalline structure.

6.1.2 Scanning Electron Microscopy

Although its spatial resolution is sometimes insufficient to resolve minute details of the sample, the classical optical microscope is a valuable instrument for studying the microstructure of materials. This is where a scanning electron microscope (SEM), an electron-beam device with higher spatial resolution, can be useful.

Primary electrons from the electron cannon are directed into a small-diameter electron probe in SEM, which is then utilized to scan the specimen. Subsequent models employ a heated filament source, and electrostatic lenses focus the electrons that are released onto the specimen. The atomic electrons in the material are stimulated by this probe, causing them to release secondary electrons as a means of interaction with the specimen. Since the energy of these secondary electrons varies, it is more challenging to concentrate them into an image with conventional electron lenses. To get around this problem, SEM uses an alternate technique of image generation that makes use of the scanning principle. A square or rectangular region of the material (referred to as a raster) can be covered by moving the electron probe over it in two perpendicular directions. By gathering the secondary electrons that are released from every location on the specimen, an image of this region

can be created. High-resolution details regarding the microstructure of materials, such as the size, shape, and orientation of individual grains as well as the existence of flaws like cracks or voids, are provided by the ensuing SEM photographs. When high-resolution imaging is needed for a variety of applications, SEM is an effective tool. It is a vital tool for scientists and engineers who want to learn more about the characteristics and behaviors of various materials because of its capacity to give comprehensive information on the microstructure of materials.

Overall, the application of scanning principles in SEM demonstrates the applicability and significance of this basic idea in numerous scientific and technological domains; it permits the creation of high-resolution images that offer insightful knowledge about the microstructure and characteristics of materials. To completely comprehend the operation of this device, we give a schematic illustration of the SEM in **Fig.34**[47].

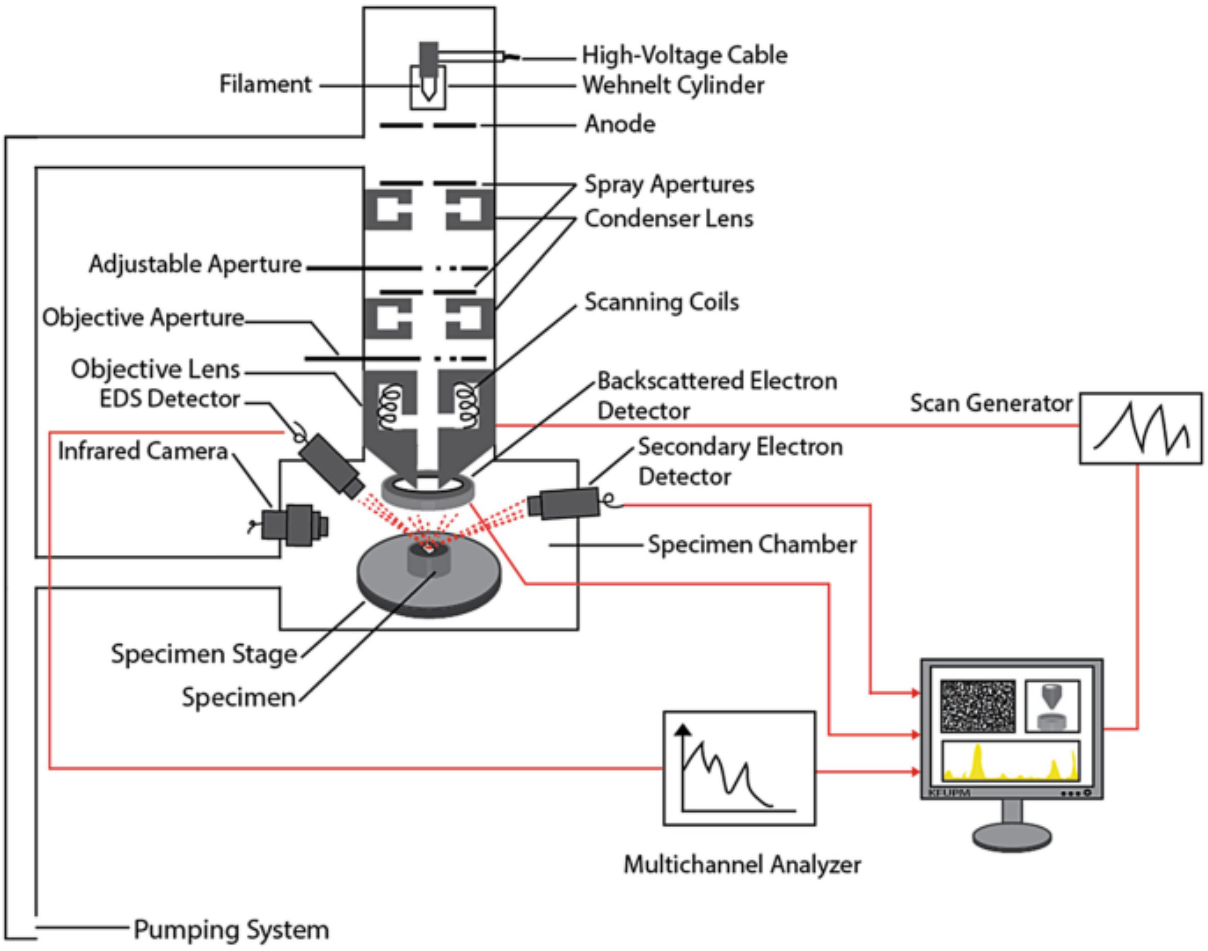

***Figure 34**. schematical representation of the SEM.*

6.1.3 Energy-dispersive X-ray spectroscopy

EDX, or Energy Dispersive X-ray spectroscopy, is a technique used to analyze the elemental composition of a material. The interaction of high-energy X-rays with the atoms of the material being studied is the foundation of the EDX principle. When an X-ray source is pointed towards a sample, it has the ability to pierce the material's surface and collide with the atoms within. This collision can excite the atoms within the sample, which implies that the atoms' inner shell electrons may be knocked off of their normal energy levels.

These ejected electrons leave behind a vacancy in the inner shell of the atoms, which must be filled by electrons from higher energy levels dropping to the lower energy level. This process releases energy in the form of an X-ray photon, which is specific to the atom that released it, resulting in an X-ray signature that is unique to each element in the sample. Thus, EDX is able to identify the elements included in the material under examination by identifying and evaluating the energy and intensity of these X-rays.

An elemental spectrum that indicates the atomic abundance and distribution in the sample is produced using the detector in an EDX system, which counts the quantity of X-rays of a specific energy that are released from the sample.

Therefore, EDX might be a helpful method to show that certain components are present in the synthesized systems. Furthermore, the validity of the synthetic technique we suggest might be verified based on the atomic abundance and distribution, for instance by calculating the stoichiometric ratios between the elements in our sample.

6.1.4 X-ray Photoelectron Spectroscopy

A very effective and potent quantitative spectroscopic method for determining a material's composition, chemical state, and electronic structure is X-ray photoelectron spectroscopy (XPS). This surface-sensitive method relies on the photoelectric effect, which happens when a substance is exposed to a beam of light, in this case, an X-ray beam. In addition to determining the elements that are present within a material and those that cover its surface, XPS may also determine the chemical state of each element as well as the material's overall electronic structure and density of electronic states.

X-ray photoelectron spectroscopy (XPS) is a valuable technique for studying chemical processes and interactions between different materials. Its ability to identify present elements and reveal which other elements they are bonded to makes it one of its main advantages. Moreover, XPS can be used for line profiling of the elemental composition across the surface or, when combined with ion-beam etching, for more in-depth profiling.

High vacuum or ultra-high vacuum conditions are necessary for XPS to detect all elements, with the exception of hydrogen and helium, and it usually requires a residual gas pressure of p ~10^{-6} Pa or less. Parts per million (ppm) detection limits are feasible with extended collecting durations and concentration at the top surface, while the detection limit of XPS is normally in the parts per thousand range.

A material is exposed to an X-ray beam that describes the chemical states of the elements derived from the measurement of the kinetic energy and the quantity of ejected electrons. This process is known as photoemission spectroscopy, and XPS is one of its members. Moreover, the electron binding energy of a released electron may be calculated using the equation below, which is an essential piece of knowledge for figuring out a material's chemical state and electronic structure. The photoelectric effect equation, which connects the energy of the X-ray photons being used, the kinetic energy of the released electrons, and the binding energy of the electrons, can be used to calculate the binding energy of the emitted electrons.

In particular, the following equation provides the electron's binding energy (BE):

$$E_{binding} = E_{Photon} - (E_{kinetic} + \varphi) \qquad (22)$$

where φ is a work function term for the particular surface of the material and accounts for the energy lost by the photoelectron as it is emitted from the bulk and absorbed by the detector; this term is constant for a given material. where $E_{binding}$ is the binding energy, E_{photon} is the energy of the X-ray photons being used, and $E_{kinetic}$ is the kinetic energy of the electron as measured by the instrument.

Based on the energy of the X-ray photons being used and the kinetic energy of the electrons being emitted, scientists can calculate the binding energy of the electrons in a material using the equation, which is effectively a conservation of energy calculation. Scientists can use this equation to calculate the binding energy of the electrons and so acquire vital information about the chemical

state and electronic structure of the material, since the energy of the X-ray at a certain wavelength is known.

6.1.5 Ultraviolet-visible spectroscopy

UV-VIS is the absorption spectroscopy or reflectance spectroscopy in the whole, neighboring visible parts of the electromagnetic spectrum as well as a portion of the ultraviolet. Due to being inexpensive and non-destructive it is widely used in experimental characterization. All that is needed is for the sample to absorb in the UV-Vis range. A light beam is passed through the sample using a UV-vis spectrophotometer, which measures the amount of light absorbed at each wavelength. The concentration of the absorbing chemical in the sample determines how much light is absorbed.

In the field of catalyst chemistry this methodology is usually used to determine the energy of band gap in semiconductors. The band gap energy of a semiconductor is a representation which describes the amount of energy which is required to excite an electron from valance band to conduction band. A good knowledge of band gap energy is vital to an accurate determination of semiconductors(catalysts) properties.

This subject was firstly introduced by Tauc in 1966 by introducing a method to estimate the energy gap of an amorphous semiconductor by taking advantage of optical adsorption spectra [48]. After that, this idea was developed by Davis and Matt [49,50].

The Tauc method is based on the assumption that the energy-dependent absorption coefficient α can be expressed by the following equation

$$(\alpha h\nu)^{1/\gamma} = B\,(h\nu - E_g) \qquad (23)$$

When B is a constant, v is the frequency of the photon, E_g is the band gap energy, and h is the Planck constant. For the direct and indirect transition band gaps, the γ factor is equal to 1/2 or 2, depending on the type of electron transfer [51].

The diffuse reflectance spectrum is typically used to calculate the band gap energy. The Kubelka-Munk function can be used to convert the measured reflectance spectra to the equivalent absorption spectra, as per the hypothesis put forward by P. Kubelka and F. Munk in 1931[52]:

$$F(R_\infty) = K/S = (1 - R_\infty)^2 / 2R_\infty \qquad (24)$$

where K and S stand for the absorption and scattering coefficients, respectively, and R is the reflectance of an infinitely thick object [53]. substituting $F(R_\infty)$ for α, yields the following form:

$$(F(R_\infty)\, h\nu)^{1/\gamma} = B\,(h\nu - E_g) \quad (25)$$

By plotting the reflectance spectrum against photon energy and finding the x-axis intersection point of the linear fit of the Tauc plot the band gap energy will be obtained. Since optical properties and the ability to generate electron- hole pairs depend on bandgap of the semiconductors, this parameter must be determined through UV-Vis characterization. Diffuse reflection (DR) can happen when solid powder is exposed to electromagnetic radiation. The diffuse reflection (DR) is the radiation that penetrates the powder sample and undergoes scattering and wavelength-dependent absorption within the nanomaterials. A portion of this radiation leaves the bulk sample in all directions. In this instance, the diffused reflection is intended to be collected by a DR accessory and directed towards a photodetector. The accessory has a spherical surface and it is known as an integrating sphere and it is coated with a white standard reflecting thin film.

Diffuse reflection (DR) measurement using a UV-Vis spectrophotometer is a common technique for figuring out particle nanomaterials' optical characteristics. These characteristics pertain to semiconducting powder nanomaterials and are represented by the bandgap energy (E_g) and absorption coefficient (K). E_g is a crucial characteristic of semiconducting nanomaterials since it establishes whether optoelectronic applications are feasible. A 1 cm^2 surfaced cylindrical holder is filled with powder samples. The powder should form a few mm thick layer for the incident light to be absorbed or scattered before reaching the back surface of the sample.

6.2 Electrochemical measurements

6.2.1 Linear Sweep Voltammetry

A useful electrochemical method for examining a sample's behavior and determining a material's electrochemical activity is linear sweep voltage measurement, or LSV. LSV is measuring the current flow that results from applying a linear voltage ramp to an electrochemical cell. Therefore, when performing LSV, it is crucial to select an adequate voltage range and scan rate to guarantee that the sample's electrochemical reaction is recorded and to fully characterize the sample. The electrolyte composition can affect the kinetics of the electrochemical reactions occurring, as well as the behavior of the sample. The electrode material selection will impact the measurement's sensitivity and selectivity. Furthermore, it is essential to maintain a constant and

controlled experimental setup, which includes regulating the sample's temperature, the electrolyte's flow rate, and the degree of agitation in the cell, in order to guarantee accurate and repeatable LSV readings. An LSV experiment can yield a voltammogram that can be used to learn more about the sample. It can also reveal information on the electrochemical activity of the sample, the existence of redox-active species, and the kinetics of the electrochemical reactions.

To put it succinctly, LSV is a useful tool for examining the electrochemical characteristics of materials and has a wide range of applications. Nevertheless, in order to guarantee that the data produced by the experiment is trustworthy and instructive, it is essential to carefully consider the experimental parameters and conditions.

In my study, the performance of as synthesized catalyst towards Oxygen evolution reaction were determined in a three-electrode configuration system at ambient condition on an electrochemical work station. Ni-foam, Pt and Ag/AgCl were used as working, counter and reference electrode respectively. Linear sweep voltammetry was performed in 10M KOH electrolyte and also 0.5M Urea-modified electrolyte to examine the catalytic activity in two different condition.

6.2.2 Tafel plot

A graphical depiction of a system's electrochemical kinetics is called a Tafel plot. It is a commonly used method in electrochemistry for figuring out how quickly electrochemical reactions are occurring at an electrode surface.

The Tafel equation, which connects the applied potential to the logarithm of the current density, serves as the foundation for the Tafel plot. Here is an expression for the Tafel equation:

$$\eta = b \log(j) \qquad (26)$$

Plotting the current density's logarithm versus the overpotential yields the Tafel plot. With a slope of b, the resulting plot is a straight line. In electrochemistry, the Tafel slope, or b, is a crucial quantity that tells us something about the kinetics of the electrochemical process that is happening.

Furthermore, since the Tafel slope and activation energy are connected by the following equation, the Tafel plot can reveal information about the reaction's activation energy.

$$b = d\eta / d(\log j) \quad (27)$$

where the temperature is T, the gas constant is R, the transfer coefficient is α, the Faraday constant is F, and the rate constant is k.

The Tafel slope can be utilized to ascertain the electrochemical reaction's mechanism because distinct mechanisms yield varying Tafel slopes. A reaction that involves the transfer of one electron is often associated with a slope of 120 mV/decade, whereas a reaction involving the transfer of two electrons is typically associated with a slope of 60 mV/decade.

All things considered, the Tafel plot and Tafel slope are crucial instruments in electrochemistry because they offer insightful data regarding the kinetics and mechanism of electrochemical events. Researchers can learn more about the underlying principles of electrochemical reactions and use that understanding to the design of more effective electrochemical devices by examining the Tafel plot and slope. The kinetics of the hydrogen evolution process (HER) on a surface in an electrochemical cell, typically a metal electrode is described by the Tafel slope. The Tafel slope in a HER system serves as a guide for the reaction mechanism's rate-limiting phase. It has to do specifically with the reaction's activation energy, which is a measurement of the energy needed for the reaction to continue. The exchange current density, a gauge of the HER reaction rate at equilibrium, is frequently estimated using the Tafel slope. A bigger Tafel slope denotes a slower rate and a higher activation energy, whereas a smaller Tafel slope implies a faster rate of HER and a lower activation energy for the reaction. The Tafel slope can also reveal details about the HER reaction's mechanism, such as whether it requires one or more electron transfer steps.

6.2.3 Stability investigation

As mentioned before, Oxygen evolution reactions are a vital part of electrochemical reactions in electro catalyst-based water splitting. As a result, most attention should be paid to overcome any barrier regarding to cell activity. This is an important subject specially in industrial sector and long-term usage of electro catalysts. Different phenomenon can affect OER process in a cell like: surface reconstruction, lattice oxygen evolution and dissolution re deposition.

A good understanding of complex reactions of the system can be fully obtained only under real and working condition. One of the best methods to achieve this goal is ex situ investigation which provides a better understanding of catalyst material. Rapid running and low-cost procedure are the other benefits of this kind of characterization. In this type of investigation, the long-term behavior of catalyst is simulated in a short scale like 30 or 36h but by applying more harsh conditions in compare to real conditions.

After running the test, study some parameters like a change in over potential can provide good information about the stability of the cell. Usually, the point that shows a significant increase in over potential can be considered as the final useful life of a cell.

7. REFERENCES

1. Solmaz, Ramazan, and Gülfeza Kardaş. "Fabrication and characterization of NiCoZn–M (M: Ag, Pdand Pt) electrocatalysts as cathode materials for electrochemical hydrogen production." international journal of hydrogen energy 36.19 (2011): 12079-12087.

2. Record, Frank A., David V. Bubenick, and Robert J. Kindya. "Acid rain information book." Acid rain informationbook. (1982).

3. Hare, Bill, et al. "Climate Action Tracker." (2015).

4. Khan, Niazul Islam, Fahim Elahi, and Md Atiqur Rahman Rana. "A study on the effects of global warming in Bangladesh." International Journal of Environmental Monitoring and Analysis 3.3 (2015): 118-121.

5. Fasullo, J. T., B. L. Otto-Bliesner, and S. Stevenson. "ENSO's changing influence on temperature, precipitation, and wildfire in a warming climate." Geophysical Research Letters 45.17 (2018): 9216-9225.

6. Mata, Teresa M., Antonio A. Martins, and Nidia S. Caetano. "Microalgae for biodiesel production and other applications: a review." Renewable and sustainable energy reviews 14.1 (2010): 217-232.

7. Wang, Shan, Aolin Lu, and Chuan-Jian Zhong. "Hydrogen production from water electrolysis: role of catalysts." Nano Convergence 8 (2021): 1-23.

8. Zhang, Haojie, et al. "Bifunctional heterostructured transition metal phosphides for efficient electrochemical water splitting." Advanced functional materials 30.34 (2020): 2003261.

9. You, Bo, and Yujie Sun. "Innovative strategies for electrocatalytic water splitting." Accounts of chemical research 51.7 (2018): 1571-1580.

10. Protsenko, Vyacheslav S. "Thermodynamic aspects of urea oxidation reaction in the context of hydrogen production by electrolysis." *International Journal of Hydrogen Energy* (2023).

11. Yang, Jinhui, et al. "Roles of cocatalysts in semiconductor-based photocatalytic hydrogen production." Philosophical Transactions of the Royal Society A: Mathematical, Physical and Engineering Sciences 371.1996 (2013): 20110430.

12. Kim, Yujin, et al. "Recent Advances in Water-Splitting Electrocatalysts Based on Electrodeposition." Materials 16.8 (2023): 3044.

13. Zhang, Peili, et al. "Dendritic core-shell nickel-iron-copper metal/metal oxide electrode for efficient electrocatalytic water oxidation." Nature Communications 9.1 (2018): 381.

14. Khalid, Mohd, et al. "Trifunctional catalytic activities of trimetallic FeCoNi alloy nanoparticles embedded in a carbon shell for efficient overall water splitting." Journal of Materials Chemistry A 8.18 (2020): 9021-9031.

15. Singh, Baghendra, et al. "Modulating electronic structure of metal-organic framework derived catalysts for electrochemical water oxidation." Coordination Chemistry Reviews 447 (2021): 214144.

16. Le Formal, Florian, et al. "A Gibeon meteorite yields a high-performance water oxidation electrocatalyst." Energy & Environmental Science 9.11 (2016): 3448-3455.

17. Chen, B. Z., et al. "Evaluation of sodium petroleum sulfonates with different molecular weights for flotation of kyanite ore." Physicochemical Problems of Mineral Processing 53.2 (2017): 956-968.

18. Zheng, Renji, et al. "Effects of crystal chemistry on sodium oleate adsorption on fluorite surface investigated by molecular dynamics simulation." Minerals Engineering 124 (2018): 77-85.

19. Kou, Tianyi, et al. "Periodic porous 3D electrodes mitigate gas bubble traffic during alkaline water electrolysis at high current densities." Advanced Energy Materials 10.46 (2020): 2002955.

20. Li, Ting, et al. "Interface engineering of core-shell Ni0. 85Se/NiTe electrocatalyst for enhanced oxygen evolution and urea oxidation reactions." Journal of Colloid and Interface Science 618 (2022): 196-205.

21. Ibraheem, Shumaila, et al. "Tellurium triggered formation of Te/Fe-NiOOH nanocubes as an efficient bifunctional electrocatalyst for overall water splitting." ACS Applied Materials & Interfaces 13.9 (2021): 10972-10978.

22. Liu, Zong, et al. "Efficient synergism of NiSe2 nanoparticle/NiO nanosheet for energy-relevant water and urea electrocatalysis." Applied Catalysis B: Environmental 276 (2020): 119165.

23. Sun, Huachuan, et al. "Rh-engineered ultrathin NiFe-LDH nanosheets enable highly-efficient overall water splitting and urea electrolysis." Applied Catalysis B: Environmental 284 (2021): 119740.

24. Zhang, Qian, et al. "Interfacial engineering of an FeOOH@ Co3O4 heterojunction for efficient overall water splitting and electrocatalytic urea oxidation." Journal of Colloid and Interface Science 623 (2022): 617-626.

25. Wang, Kaili, et al. "Engineering NiF3/Ni2P heterojunction as efficient electrocatalysts for urea oxidation and splitting." Chemical Engineering Journal 427 (2022): 130865.

26. Wang, Chao, et al. "Bimetal Schottky heterojunction boosting energy-saving hydrogen production from alkaline water via urea electrocatalysis." Advanced Functional Materials 30.21 (2020): 2000556.

27. Liu, Yanbiao, Guandao Gao, and Chad D. Vecitis. "Prospects of an electroactive carbon nanotube membrane toward environmental applications." Accounts of Chemical Research 53.12 (2020): 2892-2902.

28. Wu, Luosheng, et al. "V8C7 decorating CoP nanosheets-assembled microspheres as trifunctional catalysts toward energy-saving electrolytic hydrogen production." Chemical Engineering Journal 399 (2020): 125728.

29. Pauling, Linus. "VII. The crystal structure of pseudobrookite." Zeitschrift für Kristallographie-Crystalline Materials 73.1-6 (1930): 97-112.

30. Bassi, Prince Saurabh, et al. "Hydrothermal grown nanoporous iron based titanate, Fe2TiO5 for light driven water splitting." ACS applied materials & interfaces 6.24 (2014): 22490-22495.

31. Guo, W. Q., et al. "Crystal structure and cation distributions in the FeTi2O5-Fe2TiO5 solid solution series." Journal of Physics: Condensed Matter 11.33 (1999): 6337.

32. Jeon, Tae Hwa, et al. "Ultra-efficient and durable photoelectrochemical water oxidation using elaborately designed hematite nanorod arrays." Nano Energy 39 (2017): 211-218.

33. Tao, Hua Bing, et al. "Identification of surface reactivity descriptor for transition metal oxides in oxygen evolution reaction." Journal of the American Chemical Society 138.31 (2016): 9978-9985.

34. Anantharaj, Sengeni, Subrata Kundu, and Suguru Noda. "“The Fe Effect”: A review unveiling the critical roles of Fe in enhancing OER activity of Ni and Co based catalysts." Nano Energy 80 (2021): 105514.

35. Yang, Xin, et al. "Ru doping boosts electrocatalytic water splitting." Dalton Transactions 51.30 (2022): 11208-11225.

36. Xu, Hui, et al. "Race on engineering noble metal single-atom electrocatalysts for water splitting." International Journal of Hydrogen Energy 47.31 (2022): 14257-14279.

37. Anantharaj, Sengeni, et al. "Strategies and perspectives to catch the missing pieces in energy-efficient hydrogen evolution reaction in alkaline media." Angewandte Chemie International Edition 60.35 (2021): 18981-19006.

38. Anantharaj, Sengeni. "Hydrogen evolution reaction on Pt and Ru in alkali with volmer-step promotors and electronic structure modulators." Current Opinion in Electrochemistry 33 (2022): 100961.

39. Li, Zhao, et al. "Boosting oxygen evolution of layered double hydroxide through electronic coupling with ultralow noble metal doping." Dalton Transactions 51.4 (2022): 1527-1532.

40. Li, Yanguang, et al. "MoS2 nanoparticles grown on graphene: an advanced catalyst for the hydrogen evolution reaction." Journal of the American Chemical Society 133.19 (2011): 7296-7299.

41. Zhang, Yongqi, et al. "Rapid synthesis of cobalt nitride nanowires: highly efficient and low-cost catalysts for oxygen evolution." Angewandte Chemie 128.30 (2016): 8812-8816.

42. Yao, Qing, et al. "Channel-rich RuCu nanosheets for pH-universal overall water splitting electrocatalysis." Angewandte Chemie 131.39 (2019): 14121-14126.

43. Yang, Hongyuan, et al. "B-doping-induced amorphization of LDH for large-current-density hydrogen evolution reaction." Applied Catalysis B: Environmental 261 (2020): 118240.

44. Melo, Mauricio A., et al. "Pseudobrookite Fe2TiO5 nanoparticles loaded with earth-abundant nanosized NiO and Co3O4 cocatalysts for photocatalytic O2 evolution via solar water splitting." ACS Applied Nano Materials 3.9 (2020): 9303-9317

45. Li, Jun, and Gengfeng Zheng. "One-dimensional earth-abundant nanomaterials for water-splitting electrocatalysts." Advanced Science 4.3 (2017): 1600380.

46. Katwal, Rishu, Richa Kothari, and Deepak Pathania. "An overview on degradation kinetics of organic dyes by photocatalysis using nanostructured electrocatalyst." Delivering Low-Carbon Biofuels with Bioproduct Recovery (2021): 195-213.

47. Ul-Hamid, Anwar, and Anwar Ul-Hamid. "Components of the SEM." A Beginners' Guide to Scanning Electron Microscopy (2018): 15-76.

48. Tauc, J., Radu Grigorovici, and Anina Vancu. "Optical properties and electronic structure of amorphous germanium." physica status solidi (b) 15.2 (1966): 627-637.

49. Davis, E. A., and NFf Mott. "Conduction in non-crystalline systems V. Conductivity, optical absorption and photoconductivity in amorphous semiconductors." Philosophical magazine 22.179 (1970): 0903-0922.

50. Mott, Nevill Francis, and Edward A. Davis. Electronic processes in non-crystalline materials. Oxford university press, 2012

51. Pankove, Jacques I. Optical processes in semiconductors. Courier Corporation, 1975.

52. Kubelka, Paul, and F. R. A. N. Z. Munk. "A contribution to the optics of pigments." Z. Tech. Phys 12.593 (1931): 193.

53. López, Rosendo, and Ricardo Gómez. "Band-gap energy estimation from diffuse reflectance measurements on sol–gel and commercial TiO_2: a comparative study." Journal of sol-gel science and technology 61 (2012): 1-7.